A BI-DIRECTIONAL ACTIVE CELL BALANCING OPTIMIZATION BASED ON STATE-OF-CHARGE ESTIMATION

A Bi-directional Active Cell Balancing Optimization Based on State-of-Charge Estimation

By

Xiaowei Zhang, B.S.

A Thesis

Submitted to the School of Graduate Studies

In Partial Fulfillment of the Requirements

For the Degree of

Master of Applied Science

McMaster University

Master of Applied Science (2017) McMaster University

(Mechanical Engineering) Hamilton, Ontario, Canada

Title:

A BI-DIRECTIONAL ACTIVE CELL BALANCING OPTIMIZATION BASED ON STATE-OF-CHARGE ESTIMATION

AUTHOR: Xiaowei Zhang

SUPERVISOR: Dr. Fengjun Yan

NUMBER OF PAGES: xiv, 117

To my parents Shihui Zhang and Jiquan Zhang. All I have and will have are only possible due to the courage you support, the confidence you teach and the endless love you give

Abstract

Recently, Electric Vehicles (EVs) have received extensive consideration since they offer a more sustainable and greener transportation alternative compared to fossil-fuel propelled vehicles. Lithium-ion batteries are increasingly being considered in EVs due to their high energy density, slow loss of charge when not in use, and for lack of hysteresis effect. Conventionally, the batteries are connected in series to achieve the load voltage requirements. However, for the batteries with intrinsic discrepancies or different initial states, cell balancing is a concern because it is the weakest cell that determines the empty point for the battery and an undercharged series cell will shorten the lifetime of the entire pack. The imbalance potential of the battery behaves as the way of State-of-Charge (SOC) mismatch and it's also temperature dependent. Therefore, in this thesis, an active cell balancing optimization was proposed and conducted in MATLAB to optimize battery unused capacity and thermal effect simultaneously based on bi-directional balancing system and pre-estimated SOC. The bi-directional balancing system was physically built based on "Fly-back" converter to compare balancing performance in discharging, idle, and plug-in charging mode. Moreover, a battery combined model worked collaboratively with robust state and parameter estimation strategies, namely Extended Kalman Filter (EKF) and Smooth Variable Structure Filter (SVSF) in order to estimate SOC for cell balancing. As a result, the proposed method can effectively optimize SOC mismatch around 2.5%. Meanwhile, more uniform temperature was achieved and the maximum temperature can be reduced about 7 ℃.

Acknowledgements

The author would like to express his gratitude to his supervisor Dr. Fengjun Yan for his supervision, guidance and financial support for this research. Many thanks to his trust and the opportunities he provides so that I can undertake this research confidently and successfully.

I genuinely thank Dr. Ryan Ahmed for providing battery aging data and conducting "Management and Control of Electric Vehicle batteries" course at the faculty of engineering which helps me quickly get into this research.

I convey special acknowledgment to Dr. Daiwei Feng and my colleague Pingjiang Huang for their kind assistance, technical expertise, and support for battery experiment. They make me realize the gap between academic research and engineering, and how to conquer it.

I would like to thank every member in PCL providing me support, help and especially friendship.

Most of all, I would like to thank my family, my mother Shihui Zhang and my father Jiquan Zhang for their endless love, encouragement and absolute confidence in me throughout my entire life. Without them, I could not reach this far.

Table of Contents

List of Figures

List of Tables

Chapter 1 : Introduction

In contemporary society, energy becomes an increasingly expensive commodity, especially fuel used for ground transportation. Due to climate change and emission issues, fossil fuels energy needs to explore new technologies able to reduce their consumptions [1]. Because of this high energy conservation and emissions reduction demand from passengers, current technologies such as controlling the in-cylinder condition and after-treatment system [2]–[5] of Internal Combustion Engines (ICE) have been implemented on the conventional vehicle. However, several manufactures such as Tesla are trying to develop a number of new solutions which make use of electric drives experimented through prototypes for medium or long term applications and in some cases already on the market. As a result, Electric Vehicles (EVs) are developed generally aiming to reduce the pollutant emissions and the energy consumption.

Recently, EVs are becoming increasingly attractive in transportation sector since they offer numerous benefits such as small environmental impact, the good energy recovering and sustain ability, and their high well-to-wheel efficiency shown in Figure 1.1. However, several electrification challenges, such as cost, range anxiety, safety, and reliability still hinder the wide adoption and mass market production of EVs. These challenges could be significantly mitigated by incorporating an advanced Battery Management System (BMS).

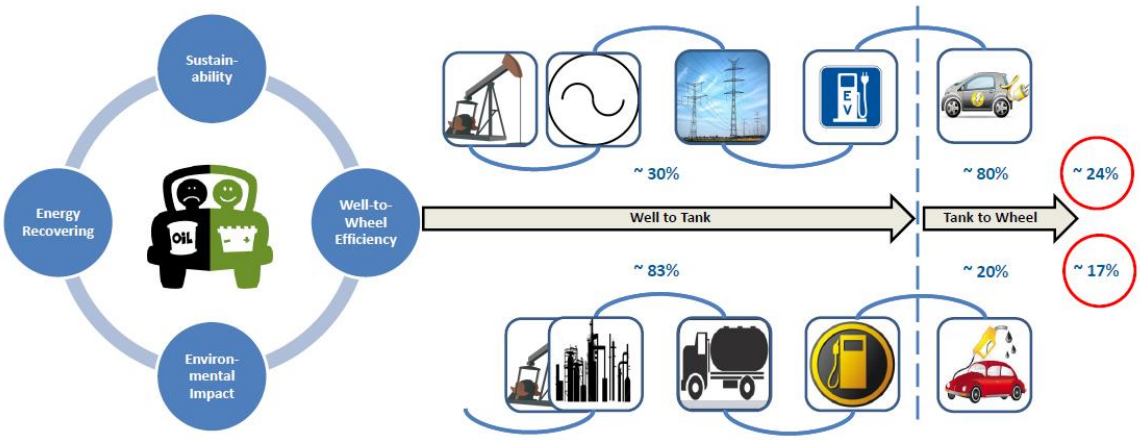

Figure 1.1 Advantages of Electric Vehicle

Since the battery pack is one of the most critical components in the EV powertrain, highly accurate monitoring, control and protection strategies have to be implemented onboard of the BMS to prolong the battery lifespan and ensure safety [6]. The BMS represents the brain of the battery; it is responsible for monitoring the battery State-of-Charge (SOC) and State-of-Health (SOH), ensuring cell-to-cell balancing, conducting thermal management, and estimating instantaneous available power. The battery SOC is one of the key variables monitored by the BMS since it is strongly linked to the vehicle driving range which is of great concern to the driver. Also, SOC is the critical parameter related to further battery application, such as battery SOC balancing. Therefore, accurate SOC estimation will ultimately improve customer satisfaction and accelerate the mass market acceptance of EVs. However, the battery SOC estimation is a relatively complex task since the battery characteristics change over time; as battery ages, it exhibits capacity and power fade, and its internal resistance increases, which in turn affects the model and the accuracy of SOC estimation. Thus, battery models have to be adaptive in order to

accommodate for the changes in battery characteristics and performance across the entire battery states of life [7].

A typical Lithium-Ion (Li-ion) battery module for EV consists of several cells in series, with several branches in parallel. Then plenty of modules compose the whole battery pack. This combination gives both the voltage and power necessary for EV and HEV applications. While common, these configurations are not as efficient as they could be. Since most battery chargers detect full charge by checking whether the voltage of the entire string of cells has reached the voltage-regulation point, individual cell SOC and voltage can vary as long as they do not exceed the limits for overvoltage protection. While discharging, since the weakest cell determines the empty point of the pack, the BMS only provides the lowest value of SOC to the driver to show how far the EV can reach. Therefore, no matter how accurate the SOC of individual cell can be estimated, the slight differences in the SOC, self-discharge rate, capacity, and temperature characteristics among the pack still have great influence on the range anxiety of EVs, even for cells that are the same model from the same manufacturer and even from the same batch of production [8].

Imbalanced cells are caused by differences in cell capacities, internal resistances, chemical degradation, and inter cell and ambient temperatures during charging and discharging. Any capacity imbalance between the modules can threaten the long-term reliability of the string as overall pack capacity is brought to the upper and lower limits of charge. In addition, cell imbalance can result in cell overcharging and overdischarging, decreasing the total storage capacity and lifetime of the unit [9]. Li-Ion cells experience two primary kinds of mismatch:

1. SOC mismatch occurs when initially-equal-capacity cells gradually diverge to contain different amounts of charge;

2. Capacity/energy (C/E) mismatch occurs when cells with different initial capacities are used together. Because cells are typically matched fairly well in the factory, SOC mismatch is the more common [10].

In order to keep battery SOC balanced, the voltage and SOC of individual cell must be monitored and estimated. When a voltage or SOC difference between cells becomes too large, a circuit can be enabled to draw more current from the higher cells or battery pack [11]. Therefore, cell balancing topology is necessary to be implemented in BMS to monitor State-of-Balance (SOB) [12] to maximize the capacity of the whole battery pack and prevent any cell of being overcharged or overdischarged.

This chapter provides a general overview of the development of electric vehicle and Li-ion battery, key issues of BMS which need to be conquered, answers for the question why accurate SOC estimation and balancing are extremely necessary for the battery pack, research motivation, scope, goals, and contributions of the thesis.

1.1 Thesis Motivation

The motivation of the thesis is driven by the urgent requirement for reducing emission and developing clean and renewable energy sources over the world. Specifically, the application of Li-ion battery for EV is considered in this thesis.

In conventional gasoline vehicles, the remaining fuel in the tank can be directly measured by using a fluid level sensor. However, in EV, the range, fuel economy, and other critical, calculated performance criteria rely greatly on SOC which is very difficult to measure. Moreover, due to the complexity of the real world driving cycles, the battery is subject to critical operation conditions, such as fast transients in the process of charging and discharging, high or low temperature when working in extreme weather. Consequently, robust estimation strategies are needed to point out SOC in order to provide the remaining energy information accurately and then improve both vehicle safety and customer satisfaction ultimately.

The battery pack can employ large high-voltage series strings of low-voltage storage units. As the pack is charged and discharged as a unit, individual cell temperature and internal chemistry characteristics can cause capacity imbalances in the form of SOC variations [9]. Therefore, based on cell level SOC estimation, cell balancing strategies are needed to be implemented onboard based on quite a lot of topologies. It should focus not only on single cell SOC equilibrium but also on balancing the discrepancies of the factors that result in imbalance problem, such as thermal effect, to further improve the range ability of EVs.

1.2 Scope and Objectives

In this thesis, the experimental data are from an extensive battery aging study which was conducted on 5.4Ah, 3.7V Lithium polymer cells. Instead of using fixed charging/discharging aging cycles at fixed C-rate, a set of real-world driving scenarios are

used to age the cells. The experimental data for healthy (Capacity = 100%) and aged cells (Capacity = 80%) are used to fit the combined model and track model parameters. As battery ages, the combined model parameters are optimized and tracked in an offline mode based on Genetic Algorithm (GA) over the entire batteries lifespan. Based on the optimized model, a state and parameter estimation strategy based on the Extended Kalman Filter (EKF) and the relatively new Smooth Variable Structure Filter (SVSF) are applied to estimate the SOC at various states of life for further SOC-based cell balancing implementation.

Considering a battery pack system consists of three Li-ion cells in series, cell balancing was formulated as optimal problem which pursues two objectives simultaneously: single cell SOC equalization and thermal balancing over the entire driving cycle. The proposed methodology was simulated in Matlab and generated the optimal solution of balancing current based on bi-directional system. Eventually, the “Fly-back” topology based balancing technique was physically implemented on the Print Circuit Board (PCB) controlled by LTC 3300 balancer and XMC 4500 microcontroller. A result analysis and comparative performance study are presented as well.

1.3 Thesis Organization

The thesis will be divided into seven chapters:

- Chapter 1: Overview of EV and Li-ion battery, thesis motivation, scope and objectives are discussed.
- Chapter 2: A literature review of battery modeling techniques, aging study, SOC estimation strategies, and cell balancing topologies is presented.

- Chapter 3: Battery combined model is introduced and identified with the help of Genetic Algorithm. The experimental and simulation configuration used for parameter identification are described.
- Chapter 4: SOC estimation algorithms are introduced and simulated with identified battery combined model, and the simulation results are analyzed. The accuracy and robustness comparison for different algorithms are discussed as well.
- Chapter 5: The details of hardware design and software programming of cell balancing physical implementation based on “Fly-back” topology are presented. The balancing performance in discharging (Dynamic Stress Test), idle and plug-in charge (Constant-Current Constant Voltage) mode are compared and analyzed.
- Chapter 6: Based on pre-estimated SOC in chapter 4 and tested balancing topology in chapter 5. A cell balancing optimization consisting of two objectives: single cell equalization and energy reduction, is proposed, formulated and solved in MATLAB coming along with simulation results. Thermal balancing performance for three cells is also described.
- Chapter 7: Conclusion and recommendation for the future research of this thesis are provided.

Chapter 2 Literature Review

2.1 Battery Modeling

EV application is a very harsh environment, with rate requirement up to and exceeding $\pm$20 C-rate and very dynamic rate profiles. This is in contrast to relatively benign portable-electronic applications with constant power output and fractional C rates [13]. In order to monitor battery characteristics, high fidelity model is a very important and challenging consideration in BMS. Numerous battery models have been proposed in the literature. The choice between these models is a trade-off between model complexity, accuracy, and parameterization effort [14]. Battery models are classified to one of the following: equivalent circuit-based models, behavioral models, and electrochemical models.

2.1.1 Behavioral Model

Behavioral models are empirical and utilize various functions to model battery dynamics. In [13], Plett has introduced a series of behavioral models, namely: the combined model, the simple model, the zero-state hysteresis model, and one state hysteresis model. These models can account for hysteresis effect, polarization time constants, and ohmic loss effects. Behavioral battery models use various empirical functions and formulas to describe the behavior of the battery cells. These models are simple to implement with fewer parameters to tune and are therefore easy to be implemented in real-time applications in a BMS. Examples are as follows:

- Shepherd model: $y_k = E_0 - Ri_k - K_i/z_k$
- Unnewehr universal model: $y_k = E_0 - Ri_k - K_i z_k$
- Nernst model: $y_k = E_0 - Ri_k - K_2 \ln z_k + K_3 \ln(1 - z_k)$

In these models, y_k is the cell terminal voltage; z_k is SOC, R is internal resistance which may change when charging or discharging, K_i is the polarization resistance chosen to make the model fit the data well.

2.1.1.1 The Combined Model

The combined model is defined as the collection of the three aforementioned models as shown below, [13]:

$$y_k = K_0 - Ri_k - \frac{K_1}{z_k} - K_2 z_k + K_3 \ln(z_k) + K_4 \ln(1 - z_k) \quad (2\text{-}1)$$

$$z_{k+1} = z_k - (\frac{\eta \Delta t}{C}) i_k \quad (2\text{-}2)$$

The combined model is relatively simple and can provide an acceptable accuracy. The parameter vector $\vec{\theta}$ consists of $K_0, K_1 K_2, K_3 K_4, R_{charging}, R_{discharging}$ which need to be estimated.

2.1.1.2 The Simple Model

The Simple model divides the combined model into two parts: one depending on SOC, and another depending only on i_k:

$$f(z_k) = K_0 - \frac{K_1}{z_k} - K_2 z_k + K_3 \ln(z_k) + K_4 \ln(1 - z_k) \quad (2\text{-}3)$$

$$f(i_k) = R i_k \quad (2\text{-}4)$$

The part depending on SOC can be overlaid by open-circuit voltage (OCV) curve as a function of SOC. So an easier and more accurate implementation of combined model is

$$z_{k+1} = z_k - (\frac{\eta \Delta t}{C}) i_k \quad (2\text{-}5)$$

$$y_k = \mathrm{OCV}(z_k) - R i_k \quad (2\text{-}6)$$

2.1.1.3 The Zero-State Hysteresis Model

The relaxation effect is another basic characteristic of the battery that emerges in the charging and discharging cycles. This effect represents the slow convergence of the battery's open-circuit voltage to its equilibrium point after hours of relaxation following charging/discharging shown as follow [15].

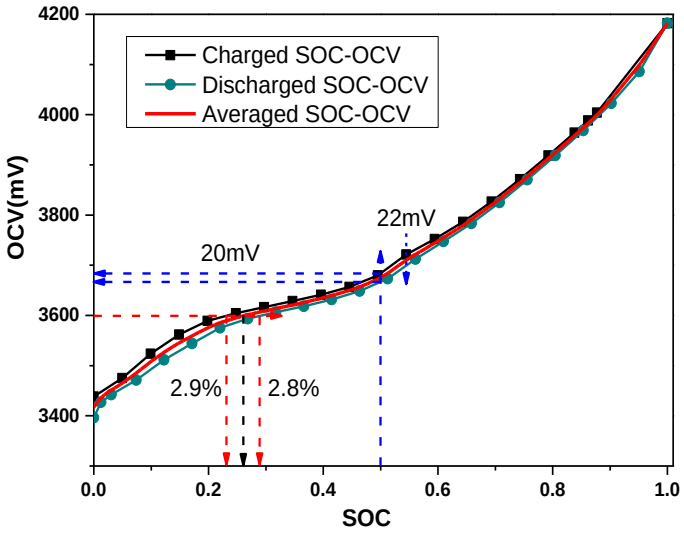

Figure 2.1 Hysteresis effect

The zero-state hysteresis model can be derived by adding another term to the simple model [13]:

$$y_k = \mathrm{OCV}(z_k) - Ri_k - s_k M(z_k) \tag{2-7}$$

Where s_k represents the sign of the current $M(z_k)$ is half the difference between the charge and discharge values. For some sufficiently small and positive value, s_k can be defined as follows:

$$s_k = \begin{cases} +1 & i_k > \varepsilon \\ -1 & i_k < -\varepsilon \\ s_{k+1} & |i_k| \le \varepsilon \end{cases} \tag{2-8}$$

The zero-state hysteresis model provided more accurate voltage estimation than simple model.

2.1.1.4 The One-State Hysteresis Model

The one-state hysteresis model is an improvement over the simple model and zero-state hysteresis model. In this model, the hysteresis effect is not a known constant value anymore but a differential equation in SOC. The hysteresis voltage can be described as follows [13]:

$$\frac{dh(z,t)}{dz} = \gamma \,\mathrm{sgn}(\dot{z})(M(z,\dot{z}) - h(z,t)) \tag{2-9}$$

Where $M(z,\dot{z})$ is a function that gives the maximum polarization due to hysteresis as a function of SOC and the rate-of-change of SOC. Specifically, $M(z,\dot{z})$ is positive for charge ($\dot{z}$ >0) and is negative for discharge ($\dot{z}$ <0). The term in front of this has a positive constant γ, which tunes the rate of decay, and $\mathrm{sgn}(\dot{z})$, which forces the equation to be stable for both charge and discharge. The overall state-space format one-state hysteresis model is

$$\begin{bmatrix} h_{k+1} \\ z_{k+1} \end{bmatrix} = \begin{bmatrix} F(i_k) & 0 \\ 0 & 1 \end{bmatrix} \begin{bmatrix} h_k \\ z_k \end{bmatrix} + \begin{bmatrix} 0 & (1-F(i_k)) \\ -\frac{\eta \Delta t}{C} & 0 \end{bmatrix} \begin{bmatrix} i_k \\ M(z,\dot{z}) \end{bmatrix} \tag{2-10}$$

$$y_k = \mathrm{OCV}(z_k) - Ri_k + h_k \tag{2-11}$$

Where $F(i_k) = \exp(-|\eta_i i_k \gamma \Delta t / C|)$.

2.1.2 Equivalent Circuit Model

Equivalent circuit models (ECM) use several RC branches such as resistors and capacitors to model the battery dynamics, charge and discharge behaviors. Due to their

simplicity, equivalent circuit models require less computational power and thus can be easily implemented onboard of a battery management system. A second-order RC branches ECM can is shown in Figure 2.2. ECM usually consists of OCV, internal resistance (denoted as R), and RC branch (R1, R2, C1, C2). What's more, adding hysteresis and temperature effect that occurs during charging and discharging process can improve the fidelity of the models.

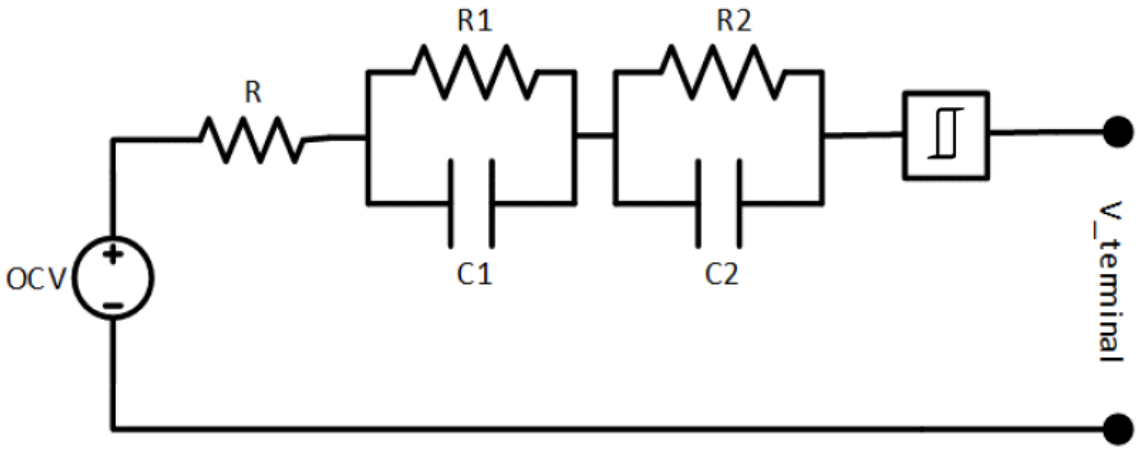

Figure 2.2 Second-order RC branch model

The choice of how many RC branches should be used is a trade-off between model complexity, accuracy, and computational efficiency. The output equations for first, second and third-order ECM are listed in Table 2.1.

Table 2.1 Output equation for first, second, and third-order ECM [16][17]

Model	**Output equations**

The first-order RC model	$U_{1,k+1}=\exp(-\Delta t/\tau_1)U_{1,k}+R_1[1-\exp(-\Delta t/\tau_1)]i_k$ $V_k=OCV(z_k)-Ri_k-U_{1,k}$
The first-order RC model with hysteresis state	$V_k=OCV(z_k)-Ri_k-U_{1,k}+h_k$
The second-order RC model	$V_k=OCV(z_k)-Ri_k-U_{1,k}-U_{2,k}$
The second-order RC model with a hysteresis state	$V_k=OCV(z_k)-Ri_k-U_{1,k}-U_{2,k}+h_k$
The third-order model RC model	$V_k=OCV(z_k)-Ri_k-U_{1,k}-U_{2,k}-U_{3,k}$
The third-order model RC model with hysteresis state	$V_k=OCV(z_k)-Ri_k-U_{1,k}-U_{2,k}-U_{3,k}+h_k$

Where $U_{1,k}$, $U_{2,k}$, and $U_{3,k}$ are the voltage of the first, second, and third order RC branches, respectively and $\tau=RC$ represents the time constant of corresponding branch.

2.1.3 Electro-chemical Model

Electro-chemical model links physical parameters to internal electrochemical dynamics of the cell. It models the Li-ion diffusion inside electrodes and electrolyte. Another advantage is the electro-chemical model can provide a better indication of battery SOH compared to the other battery models. However, it's very hard to obtain the many required physical parameters on a cell-by-cell basis in a high-volume consumer product and need model reduction [18]. In [19][20], Dr. Ahmed has analyzed typical Li-ion battery physical structure and diffusion dynamic shown in Figure 2.3 and model reduction has been conducted by generating several assumptions. However, the model is still reliable to be

applied for control and estimation purposes, such as SOC and SOH estimation and is validated by using real-world driving cycles.

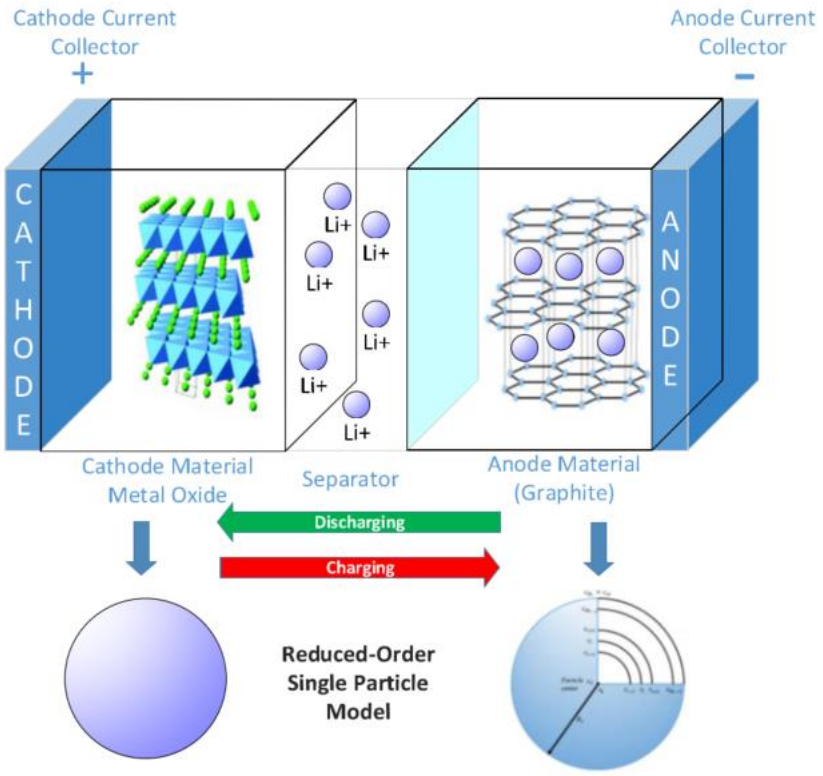

Figure 2.3 Li-ion battery structure and the reduced-order model assumption [19]

The overall state-space equations of reduced-order electro-chemical model can be described as

$$\dot{c}_s = Ac_s + Bu \tag{2-12}$$

$$c_{se} = c_{sM_r} = c_{sM_{r-1}} - \frac{\alpha_2}{\alpha_1} J_{Li} \tag{2-13}$$

Where $A=\alpha_1\begin{bmatrix} -2 & 2 & 0 & \cdots & 0 & \\ 1/2 & -2 & 3/2 & \cdots & 0 & \\ 0 & 2/3 & -2 & \cdots & 0 & \\ \vdots & & & \ddots & & \\ & & & -2 & \frac{M_r-2}{M_r-3} & 0 \\ 0 & 0 & 0 & \frac{M_r-3}{M_r-2} & -2 & \frac{M_r-1}{M_r-2} \\ & & & 0 & \frac{M_r-2}{M_r-1} & \frac{2-M_r}{M_r-1} \end{bmatrix}$, $B=\alpha_2\begin{bmatrix} 0 \\ 0 \\ \vdots \\ -\left(\frac{M_r}{M_r-1}\right) \end{bmatrix}$.

And $\alpha_1=D_s/\delta r^2$, $\alpha_2=1/(\mathrm{F}\alpha_s\delta r)$.

The single spherical particle is divided into M_{r-1} shells and shown inFigure 2.4. The parameters nomenclature and units are shown in Table 2.2.

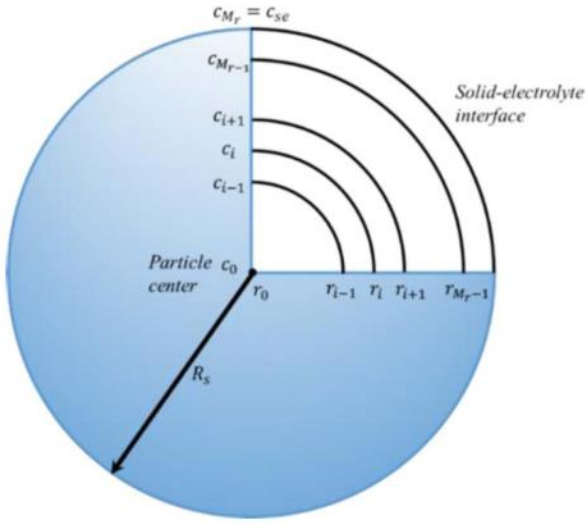

Figure 2.4 Spherical particle of radius Rs discretized into Mr shells

Table 2.2 Electro-chemical model parameters nomenclature and units [19]

Parameters	Name	Unit
c_s	solid concentration	$mol \bullet cm^{-3}$
c_{se}	concentration at the solid electrolyte interface	$mol \bullet cm^{-3}$
D_s	diffusion coefficient	/
J_{Li}	Butler-Volmer current	$A \bullet cm^{-3}$
r	Radius of the shell	cm
F	Faraday's constant	$C \bullet mol^{-1}$

This model has one input, one output, and $M_{r\text{-}1}$ states representing the shells surface concentrations. The model input u is the Butler-Volmer current (J_{Li}) which is a function of the solid-electrolyte surface concentration (c_{se}) and the total current (I). The output of this model is the solid concentration at the solid-electrolyte interface (c_{se}).

2.2 Battery Aging Study

Numerous research studies on battery aging and SOH estimation have been presented in the literature [21][22][23][24]. Based on a ninth-order polynomial model, Stamps has implemented a hybrid estimation algorithm and discrete filtering of batch estimation to predict the capacity fade and the change of inner resistance in Li-ion batteries [25]. Eric utilized capacity-based SOC measurements to compare the capacity and internal discharge resistance at various battery states of life [26]. Various research papers have

introduced aging analysis using Electrochemical Impedance Spectrometry (EIS) technique. Saha has analyzed shifts in EIS data (such as battery impedance) based on equivalent electric circuit parameters to predict the aging process [27]. Aging has been characterized in reduced-order electrochemical-based battery models, by tracking growth in the Solid Electrolyte Interface (SEI) layer in [19].

2.3 State-of-Charge (SOC) Determination

The most important responsibility of the BMS is to accurately estimate the SOC because it cannot be measured directly but provides range information and battery performance for the driver. Several proposed SOC determination methods are discussed in this section.

2.3.1 Coulomb Counting

The most widely used method for calculating SOC is called Coulomb counting. The method is also known as book keeping, current integration is performed and is compared to the nominal battery capacity thus SOC can be calculated. It depends on the integrating all charging and discharging currents [28]. If the initial SOC is known and the Coulomb efficiency is 100%, the value of the current integral is the direct indicator for the SOC, and it can be described as follow [14]:

$$SOC(t) = SOC_0 - \frac{1}{C}\int_0^t \eta_i i(\tau) d\tau \qquad (2\text{-}14)$$

Where C is the nominal capacity, η is the Coulomb efficiency, $i(\tau)$ is the instantaneous cell current, and t is the time. Coulomb counting is very simple to be implemented and can be applied to all battery chemistries.

However, this method still has several disadvantages. Such that:

- Open-loop method and measurement error can cause drift [29].
- Error accumulation occurs (due to sensor noise and inaccuracies) over time due to integration.
- A complete charge and discharge has to be conducted which limits its practical applications.
- Accurate initial SOC is needed to set up a calculation starting point in order to provide an acceptable accuracy.
- Highly depends on cell temperature, charge/discharge efficiency, and capacity degradation due to cycling which affects the accuracy of the Coulomb counting technique [17].

In order to conquer there problems, the enhanced coulomb counting method by considering charging and operating efficiencies is proposed to improve the SOC and SOH estimation accuracy [30].

2.3.2 Terminal Voltage – SOC

Based on the measurement of terminal voltage, SOC can be directly found a specific value through look-up tables, respectively. However, this method extremely suffers from inaccuracy due to the effect of temperature, battery aging and C-rate [17].

2.3.3 OCV – SOC

The OCV is a measure of the electro-motive force (EMF) of the battery, which is known to have a monotonic relationship with the SOC of the battery, hence, estimating SOC must have been a straightforward, voltage-look-up process. Furthermore, this method indicates that the relationship between OCV and SOC is stable over temperature changes and battery aging [31]. Therefore, it can be used in different chemistries, temperature, and aging. However, this method cannot be used for dynamic estimation and implemented during vehicle runtime since it requires the battery to rest completely after charging/discharging. Another issue is that it's very challenging to accurately estimate SOC in the middle part of the OCV-SOC curve due to flat voltage regions where one OCV corresponds several SOC. The relationship between OCV and SOC is shown in Figure 2.5.

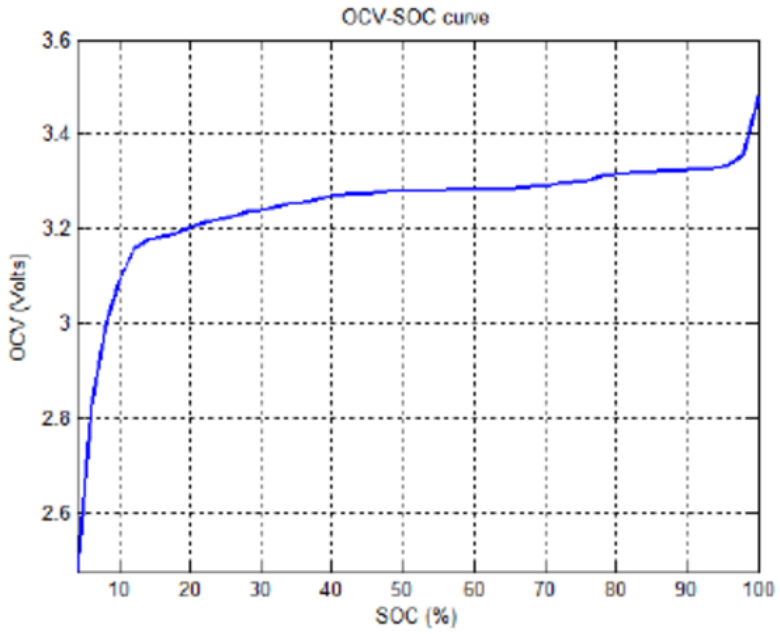

Figure 2.5 Open Circuit Voltage Vs State-of-Charge

2.3.4 Impedance Measurement

A summary of impedance measurements for determination of the SOC or SOH is presented in [32]. This method needs to set up a baseline by measuring battery impedance by exciting the battery at a range of frequencies and then SOC can be inferred based on the measured impedance, respectively [33].

2.3.5 Filter-based Estimation

Previously mentioned SOC determination methods are open-loop estimation techniques. If the estimation result drifts from the true value due to noise, temperature and battery aging effect, it cannot be recalibrated by itself. Filter-based estimation strategies are used to extract information from model to estimate one or more states in the system and

correct the final result based on the measurements from the sensor. This method can be used in the linear or nonlinear system with model uncertainty and sensor noise. Kalman Filter (KF) based estimation strategies are most widely used in SOC estimation because not only it is optimal for linear system with Gaussian noise, but also it can be easily implemented on board due to the acceptable algorithm structure and calculation time. However, in the real world situation, the battery system may not be linear anymore. Therefore, several advanced KF based filters such as the Extended Kalman Filter, the Sigma-point Kalman Filter (SPKF), unscented Kalman Filter (UKF) and Cubature Kalman Filter (CKF) are presented in [29], [34]–[38], sometimes with adaptive law [39]. These estimation strategies improve the performance of conventional KF and handling nonlinear system very well. However, it's not the optimal solution anymore. Therefore, the choices between these strategies depend on different applications and models. Another relatively new filter, SVSF, is presented in [40]. SVSF is a model based robust state estimation method that benefits from the robustness and chattering suppression characteristics of the sliding mode system [41]. It can be used to estimate SOC under model uncertainty and noisy conditions.

2.4 Cell Balancing Topologies

Lithium-ion battery chemistries cannot be overcharged without damaging active materials. The electrolyte breakdown voltage is precariously close to the fully charged terminal voltage, typically in the range of 4.1 to 4.3 volts/cell. Therefore, careful monitoring and controls must be implemented to avoid any single cell from experiencing an overvoltage due to excessive charging [42]. Cell imbalance, shown in Figure 2.6, in

battery systems is very important matter in the battery system life because without the balancing system, the individual cell voltages will drift apart over time. The capacity of the total pack will also decrease more quickly during operation then fail the battery system [43]. There are several internal and external sources that lead to cell imbalance problem. Internal sources include manufacturing differences such like the variance in initial capacities, Columbic efficiencies, internal impedance and self-discharge rate [44]. These differences may be magnified over time. While external sources mainly result from the different operation conditions of every individual cell such as location. The different location will cause different temperature effect on cells. For example, generally, inner cells are hard to release heat and therefore will have a higher temperature than outer cells. Then the individual cell will perform different charging or discharging behaviors.

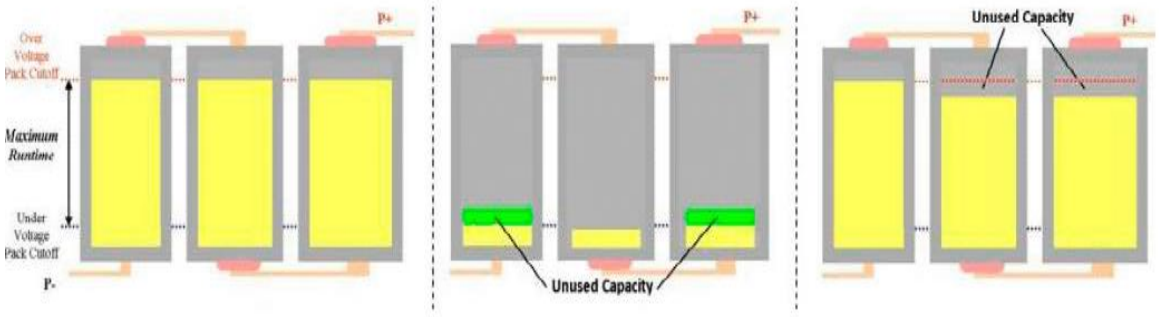

Figure 2.6 Cell imbalance problem

The balancing topologies need to conquer these problems. They can be classified as passive and active balancing shown in Figure 2.7 [44]. A comparison study can be found in [45].

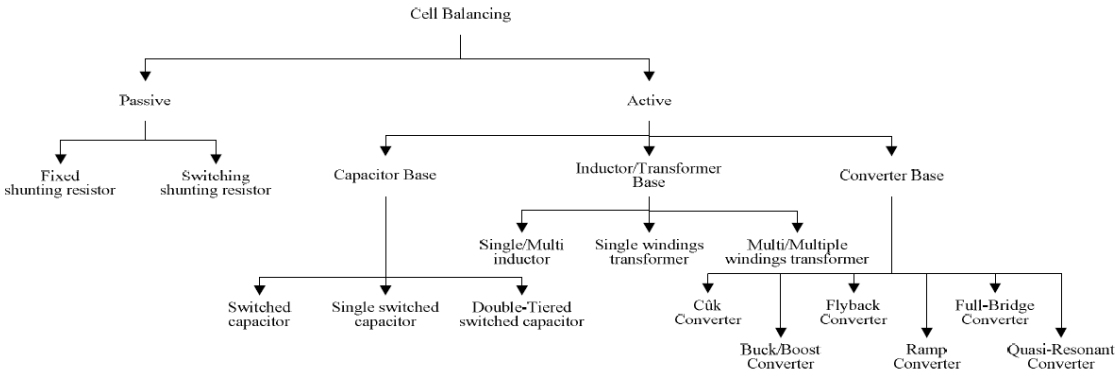

Figure 2.7 Cell balancing topologies

2.4.1 Passive Cell Balancing Topologies

In passive cell balancing topologies, excess energy can be extracted from the cells and consumed in heat. Shunting resistor methods are the most straightforward equalization concept and it based on discharging the higher voltage cells by bypass resistors until the lower voltage cells to be the same voltage level. There are two sub-categories shunting resistor methods: fixed shunt resistor and controlled shunt resistor [44].

The fixed shunt resistor method, which is shown in Figure 2.8, uses resistors to continually bypass the current for the entire battery pack and the resistors can be adjusted to limit cell voltage. However, this method can be only used for the Lead-acid and Nickel based battery since they may go through the overcharge conditions without damage [42]. The advantages of this method are that it's very easy to implement and low cost but the energy is continually wasted in heat.

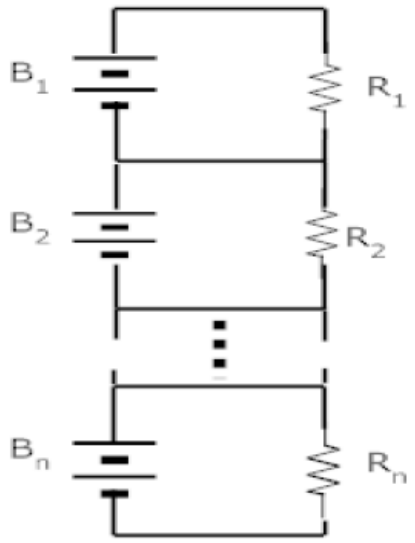

Figure 2.8 Fixed shunting resistor method

The controlled shunting resistor method can also dissipate energy through resistors not continually but controlled by using switches or relays. It can decide which resistor will be shunted depending on imbalance condition from the sensors. This method is more efficient, reliable and simple than fixed resistor method [44]. What's more, it can be used for Li-ion battery. This topology is shown in Figure 2.9.

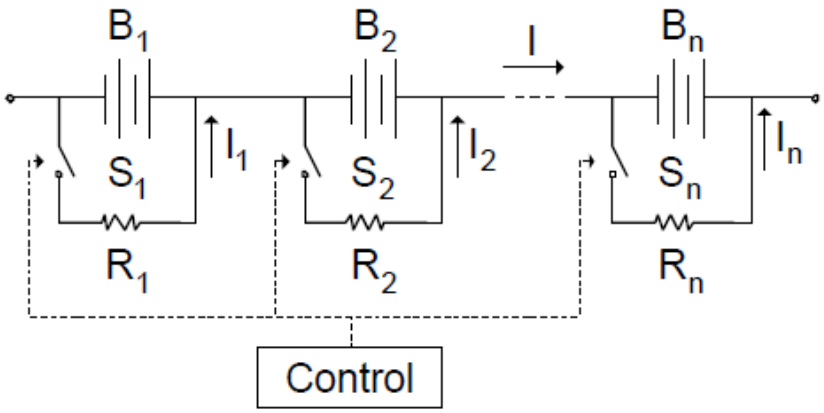

Figure 2.9 Controlled shunting resistor method

Passive cell balancing topologies are widely used in modern vehicle factory since they are low cost and don't need complex control strategies. However, the disadvantages of the shunting method are the requirement for large power dissipating resistors, high current switches, and thermal management requirements. This method is best suited for systems that are often charged with small charge currents [42].

2.4.2 Active Cell Balancing Topologies

Compared to passive cell balancing method, active cell balancing methods employ an active charge shuttling element or voltage or current converters to move energy from one cell to another instead of moving out of battery pack. It can transfer energy from cell to cell, cell to pack, pack to cell and bidirectionally [46]. These devices can be either analog or digitally controlled. The active cell balancing methods can be classified based on energy transfer devices which are capacitor, transformer, and converter.

2.4.2.1 Capacitor Based Topologies

Capacitive cell balancing, also known as "Charge Shuttling" equalization, utilize basically an external energy storage devices, the capacitor for shuttling the energy between the pack cells so as to the balancing [47]. This method includes basic switched capacitor, single switched capacitor and double-tiered capacitor topologies [9][43][48][49].

The basic switched capacitor topology is shown in Figure 2.10. In this topology, 2n switches and n-1 capacitors are needed in order to balance n cells. Basically, the capacitor constantly switches between the adjacent cells, thereby transfering charge from higher charged cell to lower charged cell. The control strategy is very simple in this topology

because it only has two states. For instance, when C1 is connected to B1, C1 and B1 are paralleled so that C1 will obtain the same voltage as B1. After this process, C1 will shunt to B2 and it will be charged or discharged to maintain the same voltage with B2 as the previous state. Therefore, after cycles and cycles, B1 and B2 will be balanced. The same thing will happen to C2 and so on. The entire battery pack can be balanced in the end.

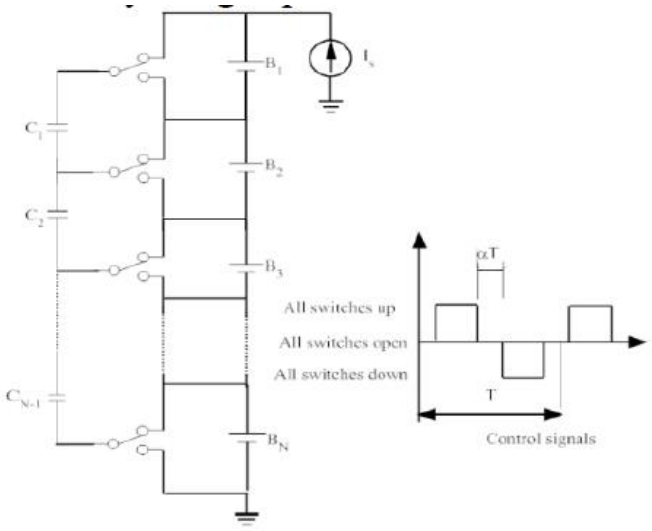

Figure 2.10 Switched capacitor topology

However, this topology takes time to balance the entire battery pack since the charge would have to travel through every cell with time and efficiency penalties. In addition, the voltage drop on switches and wire cannot be ignored. Therefore, if the voltage difference of adjacent cell is small, it very difficult to balance. In order to conquer this problem, a zero-current switching method is proposed in [50]. It realizes the zero-voltage gap between cells and provides maximum energy recovery in a series battery system by designing a resonant switched capacitor cell balancing system. So it can overcome the

drawback of conduction loss, switching loss and finite voltage difference among battery cells.

The single switched capacitor topology is kind of derivation of the switched capacitor but it only uses one capacitor to transfer charge between every cell. In this topology, n+5 switches are needed to balance n cells. The control strategy is simple as well. The controller selected the higher voltage cell and lower voltage cell and the corresponding switches for transfer charge between this two cells. However, if the simple control strategy is used, the speed of balancing is only 1/n of the switched capacitor method [43]. This topology is presented in Figure 2.11.

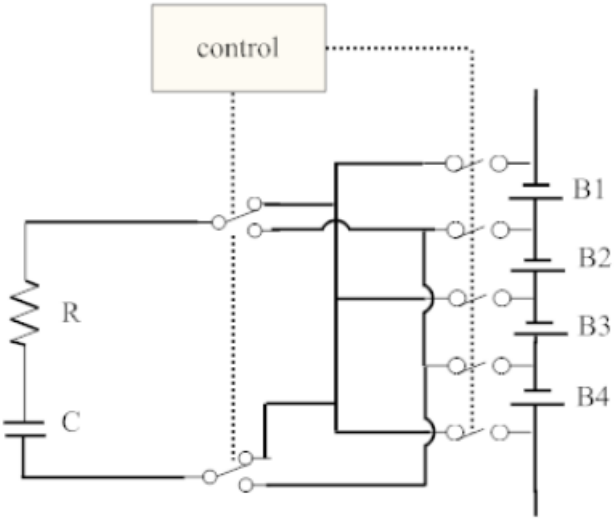

Figure 2.11 Single switched capacitor topology

The double-tiered capacitor topology is also a derivation of switched capacitor method and it is shown in Figure 2.12. In this method, a new capacitor has been added to bridge the capacitor in the first tier. This improvement can help the system speed up

balancing since batteries have opportunities to exchange charge through not only a first tier capacitor but also the second-tier bridging capacitors. As a result, the equilibrium time can be reduced significantly.

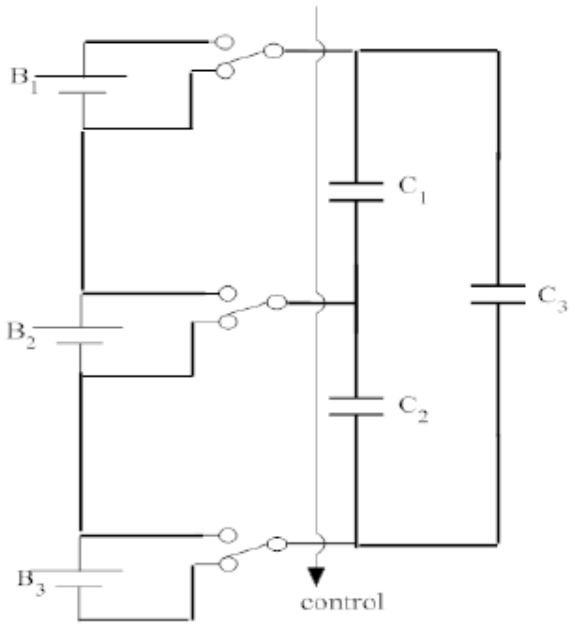

Figure 2.12 Double-tiered capacitor topology

2.4.2.2 Transformer Based Topologies

In this method, the energy can be transferred from a cell or group to another cell or group through transformers. It provides an acceptable balancing time but the disadvantages are relatively high cost and complexity. There are two specific methods which are the switched transformer, the shared transformer and multiple transformers [41] [43].

The switched transformer method is shown in Figure 2.13. It shares the same switching topology. Current I is taken from the entire pack and is switched into transformer T. The transformer output is rectified through diode D and delivered into cell Bn, which is

determined by the setting of switches S (MOSFET). Electronic control is required to select the target cell and set switches S.

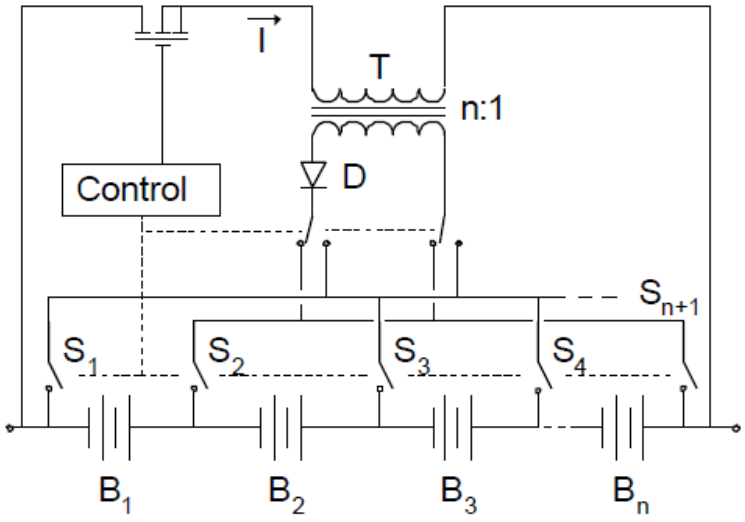

Figure 2.13 Switched transformer topology

The shared transformer topology has a single magnetic core with one primary windings and multiple secondary taps for each cell (Figure 2.14). The current I is also extracted from the entire battery pack and switched into primary, then induced current can be charged into each cell based on the reactance. The lower voltage cell will have lower reactance. Therefore, it will get the most induced current. As a result, the charging current for each cell is proportional its relative SOC.

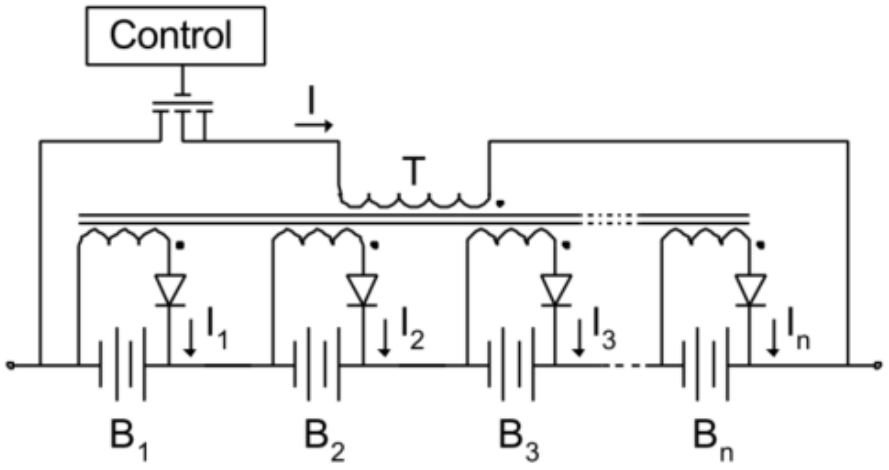

Figure 2.14 The shared transformer topology

The multiple transformers topology is shown in Figure 2.15. It can be used with the same result by coupling multiple primary winds instead of a single core. Compared to the shared transformer method, this topology is better for modular design and battery pack extension without altering the host controller although it is still expensive.

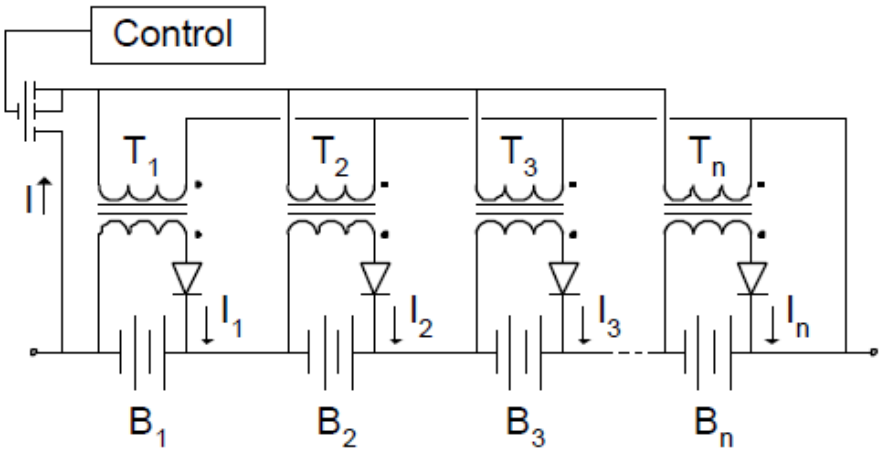

Figure 2.15 Multiple transformer topology

2.4.2.3 Converter Based Topologies

Cell balancing utilizes energy conversion devices to transfer energy. The associated energy converters can be bidirectional for both charging or discharging [42][44][51]. The energy converter falls in several categories such as Ramp converter, Buck/Boost converter, and “Fly-back” converter.

Ramp converter topology as shown in Figure 2.16 uses the similar principle with the shared transformer method and it is also an improvement on the shared transformer balancing circuit. Ramp converter only requires one secondary wind for each pair of cells instead of one cell. The ramped current shape determines the name of this topology and can summarize as two cycles [52]. At the first half cycle, most of the current is used to charge the odd number of lowest voltage cells while on the other half cycle, most of the current is used to charge the even number lowest voltage cells.

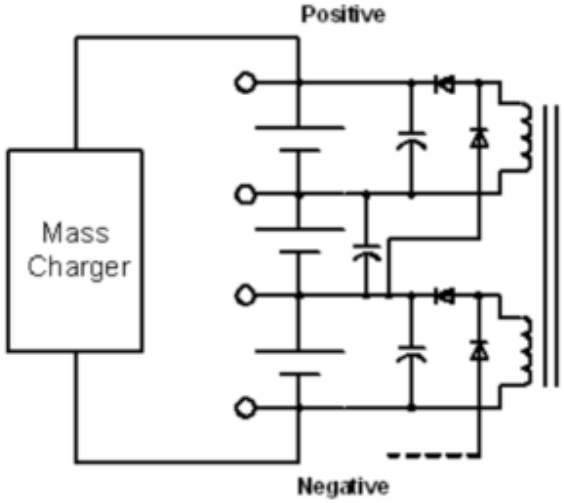

Figure 2.16 Ramp converter topology

Buck/Boost converters are widely used in cell balancing system and shown in Figure 2.17. It can be step-down (Buck), step-up (Boost). Combining Buck and Boost converter, it can realize bidirectional energy transfer such that removing excess energy from the highest voltage cell to the DC link, the storage element and retransfer the energy to the lower cells.

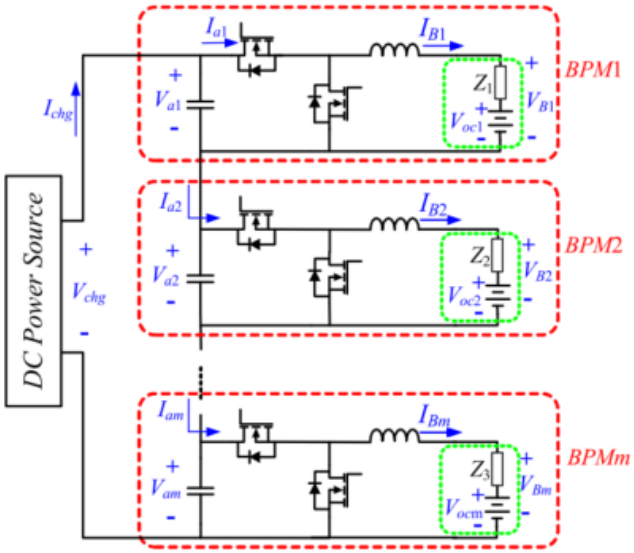

Figure 2.17 Buck/Boost converter topology

"Fly-back" converter as shown in Figure 2.18 is also based on transformer but works in a different way. Both sides of windings don't work as a transformer anymore but as inductors. The transformer can be shared windings or multiple windings and can transfer energy bidirectional [53]. The disadvantages of this topology are uniformity of the multi windings as well the magnetic losses.

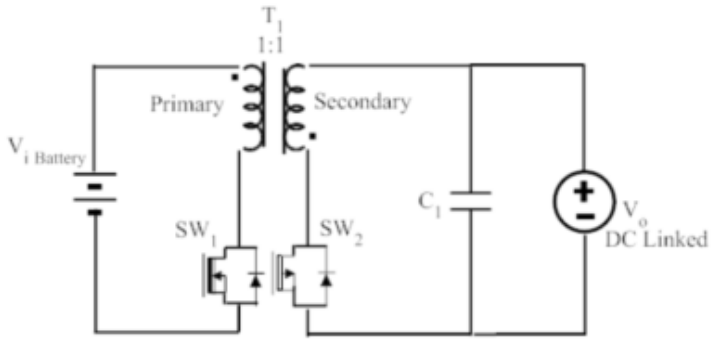

Figure 2.18 Flyback converter Topology

For transformer and converter based balancing topology, intelligent control can be applied to the system to significantly reduce the balancing time and improve the energy transfer efficiency [53]–[57].

Chapter 3 : Battery Modeling

3.1 The Combined Model

Behavioral battery models use various empirical functions and formulas to describe the behavior of the battery cells. These models are simple to implement with fewer parameters to tune and are therefore easy to be implemented in real-time applications in a BMS. Examples are as follows.

- Shepherd model: $y_k = E_0 - Ri_k - K_i/z_k$
- Unnewehr universal model: $y_k = E_0 - Ri_k - K_i z_k$
- Nernst model: $y_k = E_0 - Ri_k - K_2 \ln z_k + K_3 \ln(1 - z_k)$

In these models, y_k is the cell terminal voltage, i_k is the input current, z_k the is SOC, R is the internal resistance which may change when charging and discharging, K_i is the polarization resistance chosen to make the model fit the data well. The combined model is defined as the collection of the three aforementioned models as:

$$y_k = K_0 - Ri_k - \frac{K_1}{z_k} - K_2 z_k + K_3 \ln(z_k) + K_4 \ln(1 - z_k) \tag{3-1}$$

$$z_{k+1} = z_k - (\frac{\eta \Delta t}{C}) i_k \tag{3-2}$$

The combined model can predict the terminal voltage through SOC and is used in this chapter since it is relatively simple and can provide an acceptable accuracy. Most importantly, it doesn't need the profile of OCV with SOC. Only the data of terminal voltage

is good enough to identify the parameters of the model. The parameter vector $\vec{\theta}$ consists of K_0, K_1, K_2, K_3, K_4, $R_{charging}$, $R_{discharging}$ which need to be estimated.

3.2 Battery Test

As shown in Figure 3.1 and Table 3.1, three benchmark driving cycles are used during the aging study and model fitting; namely, an Urban Dynamometer Driving Schedule (UDDS), a light duty driving cycle for high speed and high load (US06), and a Highway Fuel Economy Test (HWFET) [58]. The UDDS driving cycle is used to simulate a city driving condition; the UF06 cycle is a high acceleration, aggressive driving cycle; the HWFET is used to characterize a highway driving condition with speed below 60 miles/hours.

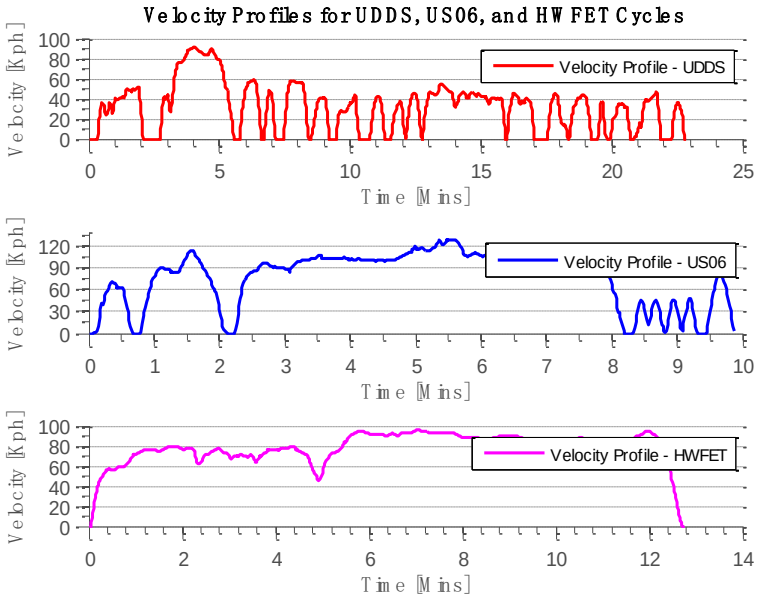

Figure 3.1 Velocity profiles for the UDDS (upper), US06 (middle), and HWFET (lower) cycles [58]

Table 3.1 Characteristics of UDDS, US06 and HWFET Driving Schedules

	Length (sec)	Distance (miles)	Average Speed (mph)
UDDS	1369	7.45	19.59
US06	596	8.01	48.37
HWFET	765	10.26	48.30

A mid-size all-EV model is modified from an existing hybrid vehicle model (Figure 3.2) and simulated in MATLAB/SimScape environment in order to generate the current profile from the velocity profile. The EV model consists of Li-ion battery pack, vehicle dynamic model, DC motor, DC-DC converter and vehicle speed controller. The aging test is interrupted by a series of reference performance test schedules to track changes in the battery performance, these tests include:

- A static capacity test at 1C, 2C, 3C, and 4C;
- Static capacity test at low C-rate (C/15 – C/25) in order to obtain the relationship between the OCV and the SOC;
- A series of UDDS, US06, and HWFET driving cycles (*Schedule A*) (that scans the entire SOC range from 90% to approximately 20%);

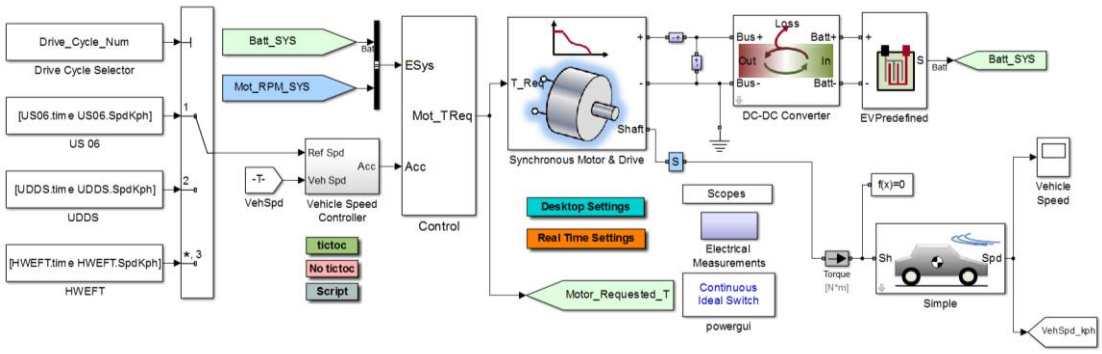

Figure 3.2 All-Electric Mid-size Sedan Simulation Model in SimScape

The current generated from the electric vehicle is converted from the pack level (Figure 3.3) to the cell level based on the battery construction. Then the cell level current profile is put into the experiment setup which includes three channel Arbin BT 2000 tester, three environmental chambers, AVL Lynx data acquisition system, AVL Lynx user-interface software and Li-ion cells to extract the terminal voltage and actual (reference) SOC. Driving Schedule A lasts approximately 290 minutes and is mixed by UDDS, US06, and HWFET test schedules. The current range of Schedule A is from -2C to 2C and covers the entire SOC from 90% to 20%. In order to demonstrate the difference in terminal voltage and SOC using the same driving schedule at different states of life, both voltage and SOC data for fresh (healthy) and aged battery at approximately 80% capacity for driving Schedule A are plotted as shown in Figure 3.4 and Figure 3.5, respectively.

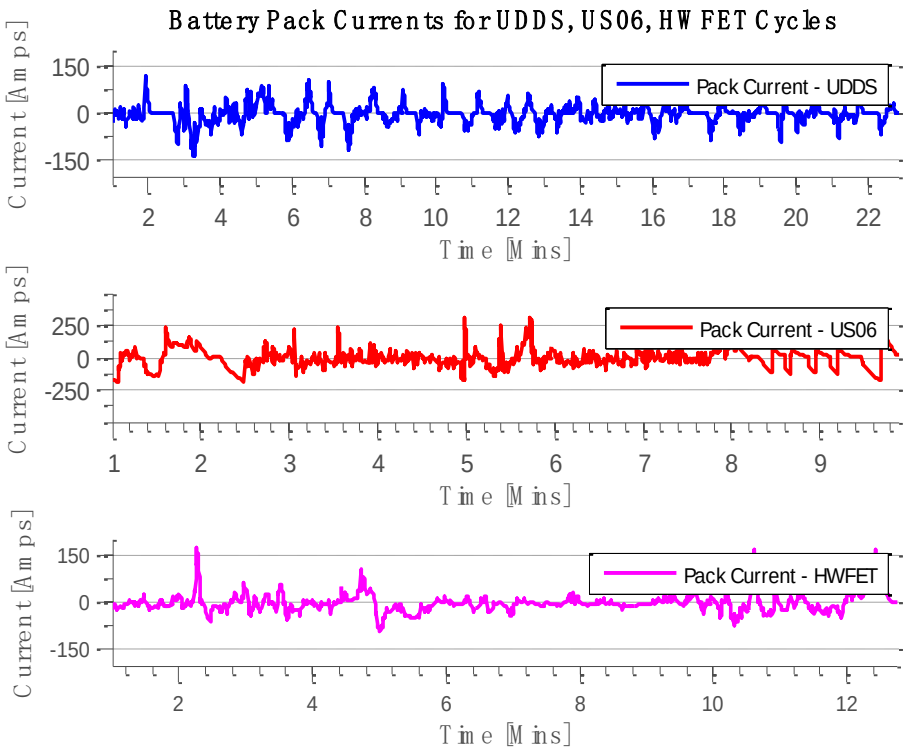

Figure 3.3 Pack current profiles for the UDDS (Upper figure), US06 (middle figure), and HWFET (lower figure) cycles

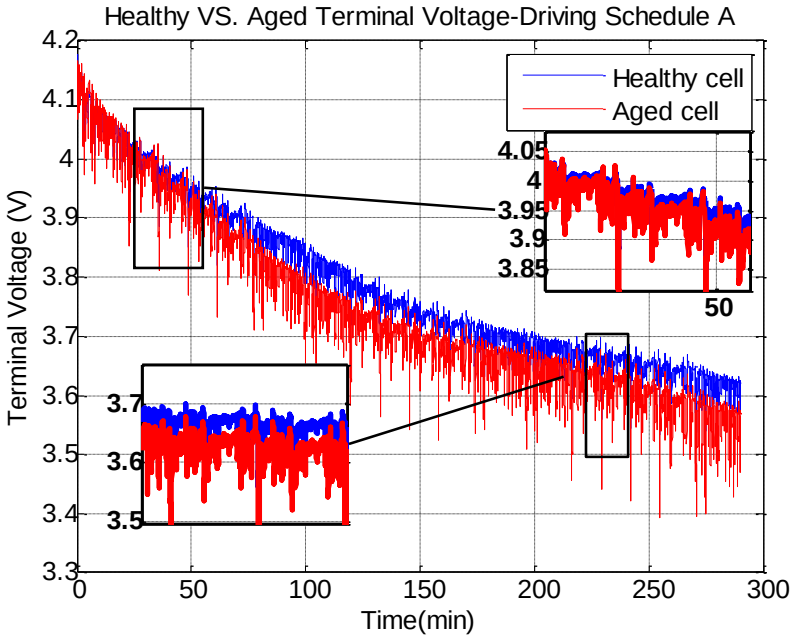

Figure 3.4 Terminal Voltage for healthy cell and aged cell at 80% capacity – Driving Schedule A

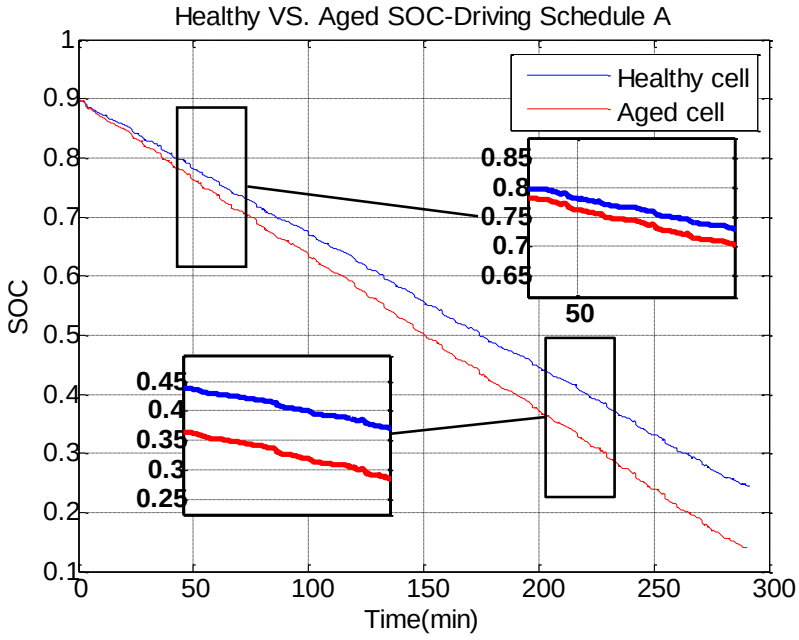

Figure 3.5 SOC for healthy cell and aged cell at 80% capacity – Driving Schedule A

As shown above, the terminal voltage and SOC of aged cell dropped more quickly than healthy cell under the same load condition. It results from the change of battery characteristics over time such as internal resistance, coulomb efficiency and capacity.

3.3 Offline Parameter Identification

In this section, the offline parameter identification using Genetic Algorithm optimization is presented. Two states of life are considered; namely: fresh (healthy) battery state (100% capacity) and aged state (80% capacity). The GA algorithm is applied to estimate battery parameters by using current and voltage data from Schedule A driving cycle. The model is simulated once for every member of the population and the terminal voltage is further compared with the experimental terminal voltage.

3.3.1 Genetic Algorithms

GA is search technique based on the evolutionary model and is used for solving constrained and unconstrained optimization problems based on a natural selection process that mimics biological evolution [59]. It has the following optimization advantages:

- GA algorithm does not require gradient calculation which is rather difficult to obtain in some complex optimization problems.
- GA can find global minima for highly nonlinear problems.

There are several definitions same as biological world such as population, parents and children. The algorithm repeatedly modifies a population of individual solutions. At each step, the algorithm randomly selects individuals from the current population and uses

them as parents to produce the children for the next generation. Over successive generations, the population evolves toward an optimal solution. The GA logical scheme is shown in Figure 3.6. The optimization procedures are:

1) The initial guess is made based on the literature for parametric values;
2) The fitness value of every population member is valuated;
3) Based on the fitness function, individuals are selected to become parents;
4) Off springs are generated from the population by crossover or mutation (Figure 3.7) ;
5) Individuals with the best fitness value are chosen to be elite and passed to the next generation;
6) Low fitness individuals from the current population are replaced by new off springs to be used in the next generation;
7) Steps are repeated until stopping criteria is reached or the maximum number of iterations.

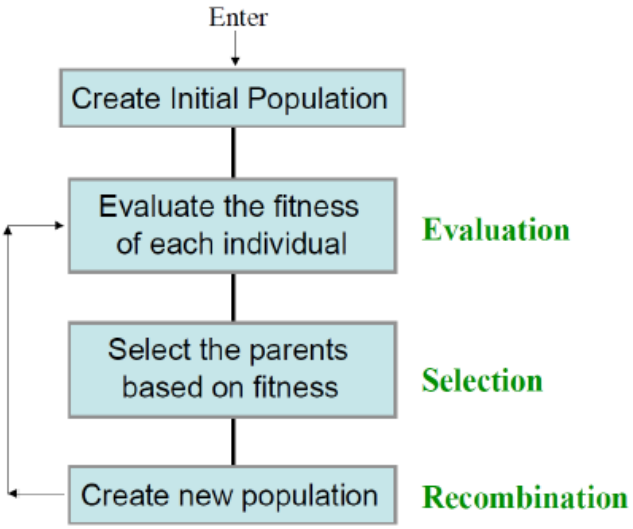

Figure 3.6 GA logical scheme

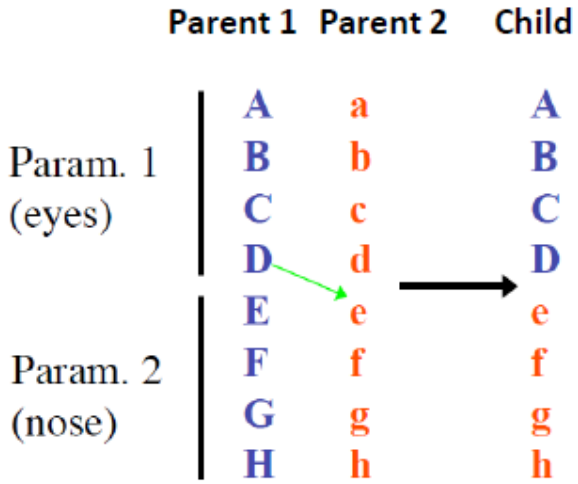

Figure 3.7 Off springs generation by crossover

The objective function is targeted at minimizing the error between the model output terminal voltage $\hat{V}(t)$ and the experimentally measured terminal voltage $V(t)$. The parameter vector $\vec{\theta}$ consists of K_0, K_1, K_2, K_3, K_4, $R_{charging}$, $R_{discharging}$ that need to be estimated. The objective function is a cumulative sum of the squared voltage error as

$$\min_{\vec{\theta}} \int_0^T (V(t) - \hat{V}(t;\vec{\theta}))^2 dt \qquad (3\text{-}3)$$

The initial value, lower bound, and upper bound of the combined model parameters are presented in Table 3.2.

Table 3.2 Parameter Initialization

	Initial value	Lower bound	Upper bound
$R_{\_charging}$	0.0177	0	0.1
$R_{\_discharging}$	0.0221	0	0.1
K0	3.5190	3	4.5
K1	0.0233	0	0.2
K2	0.0212	0	0.2
K3	-0.0867	-0.2	0.2
K4	-0.2950	-0.5	0.1

3.3.2 Optimization Results

The GA optimization is used to optimize the battery combined model parameters based on the voltage and current experimental data. It is set to five runs and 2500 population size shown in Figure 3.8. The algorithm is conducted on a mobile workstation with 2.40 GHz, Dual-core i7-5500U processor.

```
options.PopInitRange = [  0 0 3 0 0 -0.2 -0.5 ;  0.1 0.1 4.5 0.2 0.2 0.2 0.1 ]
options.PopulationSize = 2500
options.Generations = 5
options.InitialPopulation = [  0.0177 0.0221 3.519 0.0233 0.0212 -0.0867 -0.295 ]
```

Figure 3.8 GA Configuration

The optimized terminal voltage vs. the actual (measured) voltage for both fresh and aged states are as shown below in Figure 3.9 and Figure 3.10, respectively. It is important to note that in this method, one set of parameters are used over the entire SOC range shown in Figure 3.11 and Figure 3.12.

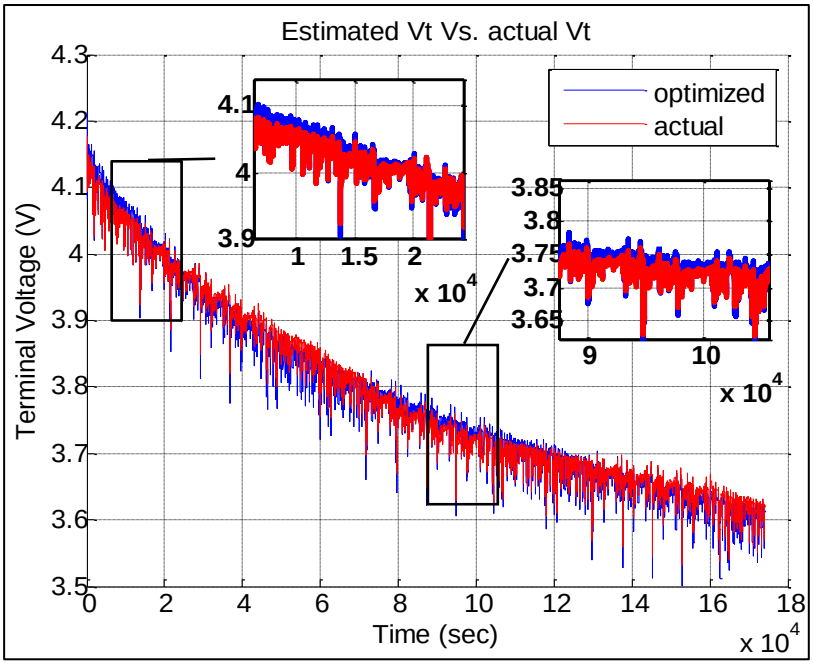

Figure 3.9 Estimated Vs. actual terminal voltage for driving Schedule A (Healthy cell)

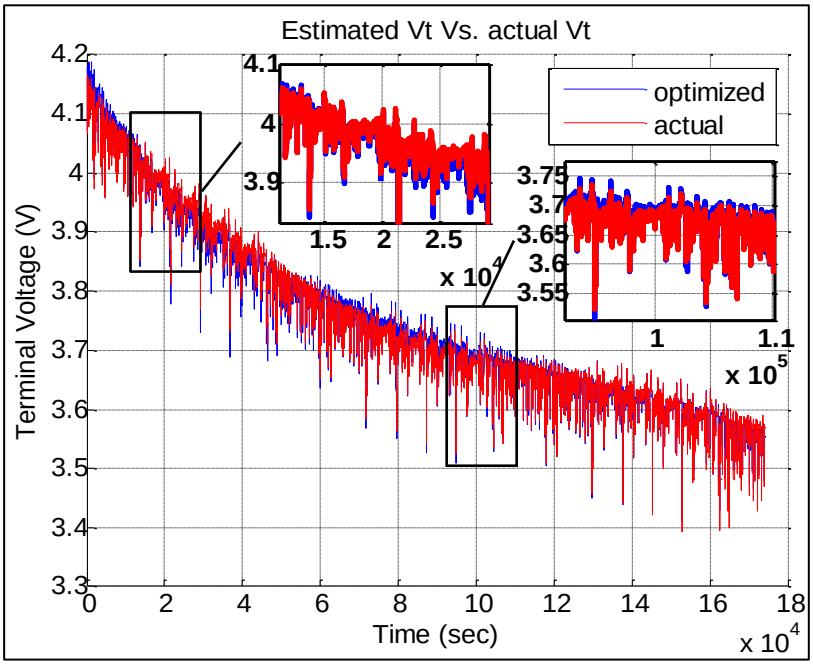

Figure 3.10 Estimated Vs. actual terminal voltage for driving Schedule A (Aged cell)

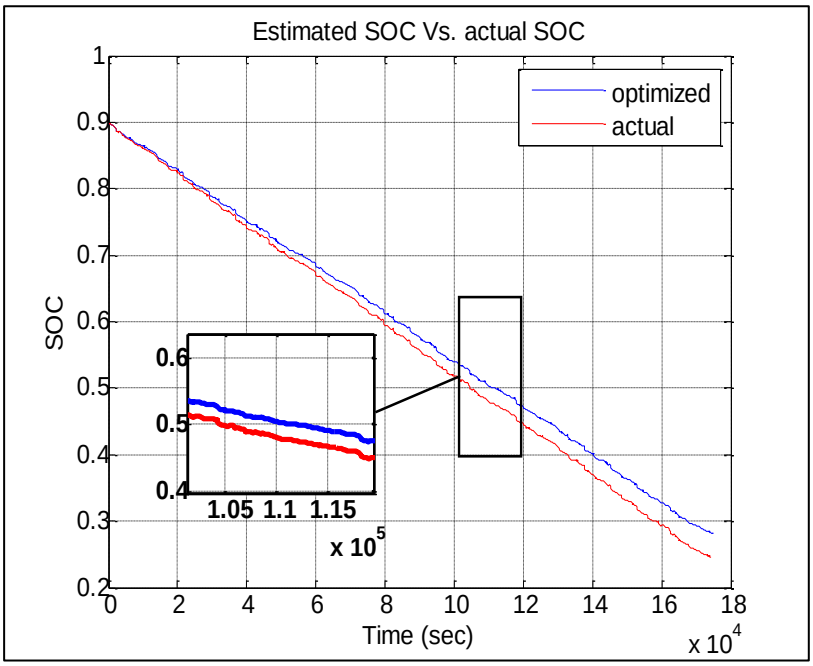

Figure 3.11 Estimated Vs. actual SOC for driving Schedule A (Healthy cell)

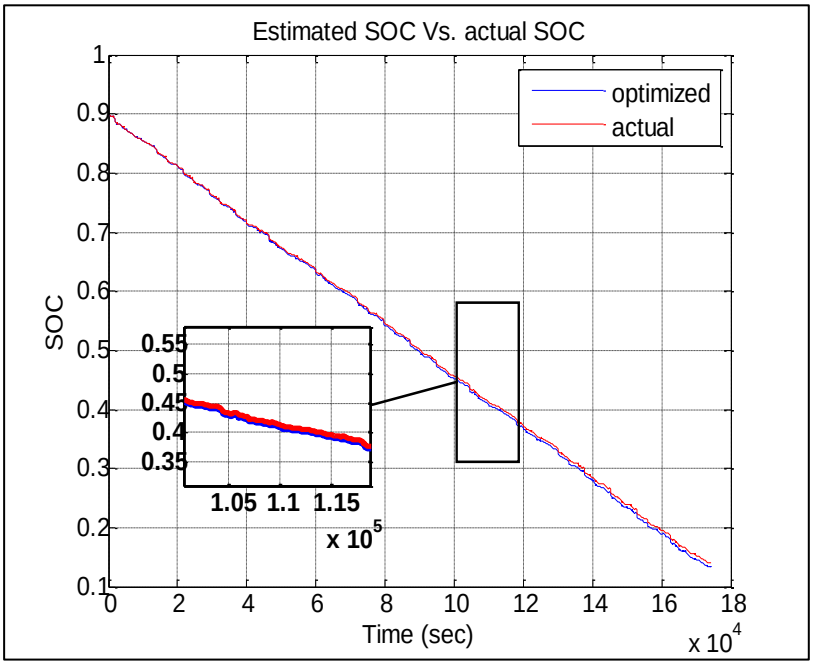

Figure 3.12 Estimated Vs. actual SOC for driving Schedule A (Aged cell)

The optimized parameters for both healthy and aged cells are as shown below in Table 3.3. The charging and discharging internal resistances: $R_{charging}, R_{discharging}$ increase over the lifespan of the battery, which reflects aging effects. Furthermore, the state estimation error variance is shown in Table 3.4. It shows that the SOC error variance of the aged cell model is smaller than the fresh cell model, which means the battery aged model is more accurate than the fresh battery model because the GA runs from the aged model and applies more populations and generations on optimizing battery aged model.

Table 3.3 Optimized Parameters

	Healthy cell	Aged cell
$R_{\_charging}$	0.0130	0.0177
$R_{\_discharging}$	0.0103	0.0165
K0	3.5190	3.5190
K1	0.0233	0.0233
K2	0.0212	0.0876
K3	-0.0666	-0.0867
K4	-0.2950	-0.3282

Table 3.4 State Estimation Error Variance

Healthy cell	Aged cell
$1.1517e^{-3}$	$3.7678e^{-6}$

Chapter 4 : State-Of-Charge Estimation

In this section, two estimation strategies are applied to the battery to extract information regarding the battery SOC based on the optimized model. The strategies are known as Extended Kalman Filter and Smooth Variable Structure Filter, which both work in a predictive-corrective form.

Estimation strategies are needed for battery SOC determination because of two reasons: Firstly, the model cannot be optimized perfectly and it contains model uncertainties. In a word, the model cannot be absolutely accurate; Secondly, the current and voltage data from real-world come with high-frequency sensor noise. Therefore, the estimation strategies are used to extract useful information hidden in model uncertainties and sensor noise, and present relative accurate and robust estimation results.

4.1 Extended Kalman Filter

Kalman Filter was developed in 1960 by R.E. Kalman. It can be used to compute hidden state variables from observation. KF is an optimal filter for the linear system with Gaussian noise since it is a computational efficiency algorithm for combing sensor noise outputs to estimate the state of a system with uncertain dynamics and present minimization of the Minimum Mean Square Error (MMSE) between the estimated state the true value. It is a multi-input and multi-output digital filter working in predictor-corrector fashion. Three factors are needed for KF: system dynamic model, control inputs and recursive measurement including noise. KF is a model based filter and it can fuse the measurement

and prediction based on your trust for each one. The algorithm work in the way of Figure 4.1.

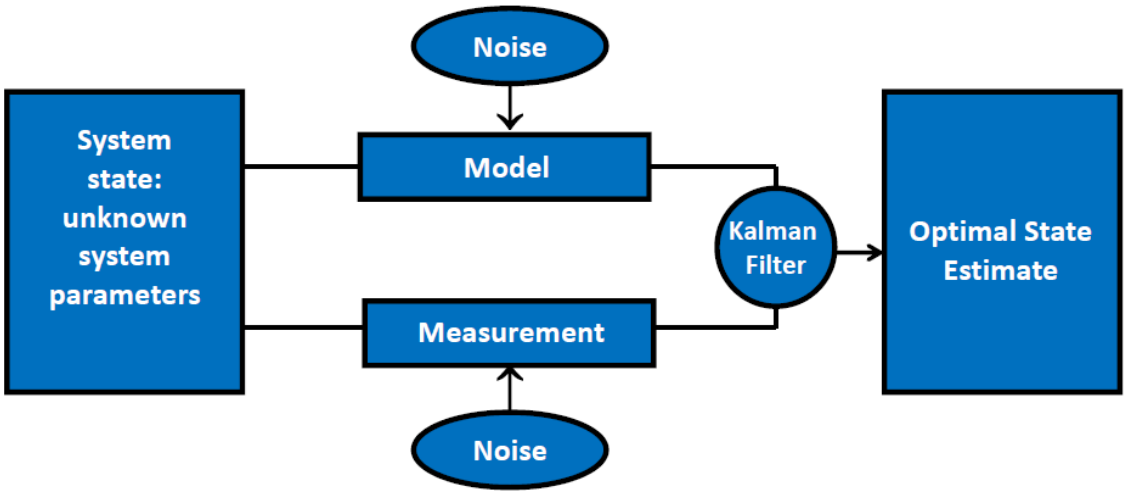

Figure 4.1 Working mode of KF

There are three important covariance matrices which can be denoted as P, Q and R. P contains estimates of the uncertainty and correlation between uncertainties of state vector components, which is regarded as parameter covariance matrix. Q is the process covariance matrix and describes the model uncertainty (system noise). R describes the measurement covariance matrix and measurement noise. Generally, these three matrices need to be initialized and tuned well depending on the system. R can be calculated based on the experimental data. However, Q cannot be recognized directly and only can be guessed approximately. The choice of small Q means dynamic model is trusted more. On the contrary, measurement is trusted more. The initialization process of these three covariance matrices can be done by trial and error, or with the help of optimization technique such as Genetic Algorithm.

Another significant variable of KF is the Kalman gain. It can determine the weighting of current measurements and estimations from the previous iteration. The Kalman gain is the optimal weighting matrix for combining new sensor data with a prior estimate (a-priori estimate) to obtain a new optimal estimate (a-posteriori). Since the estimated state is not exact, the parameter (state error) covariance matrix P needs to be calculated and regularly updated. The goal of Kalman gain is to minimize the state error covariance matrix.

KF is a two-step process: prediction and correction as shown in Figure 4.2. The prediction process presents a-priori estimation based on the dynamic model. The correction step makes corrections to an estimate, based on new information obtained from sensor measurements.

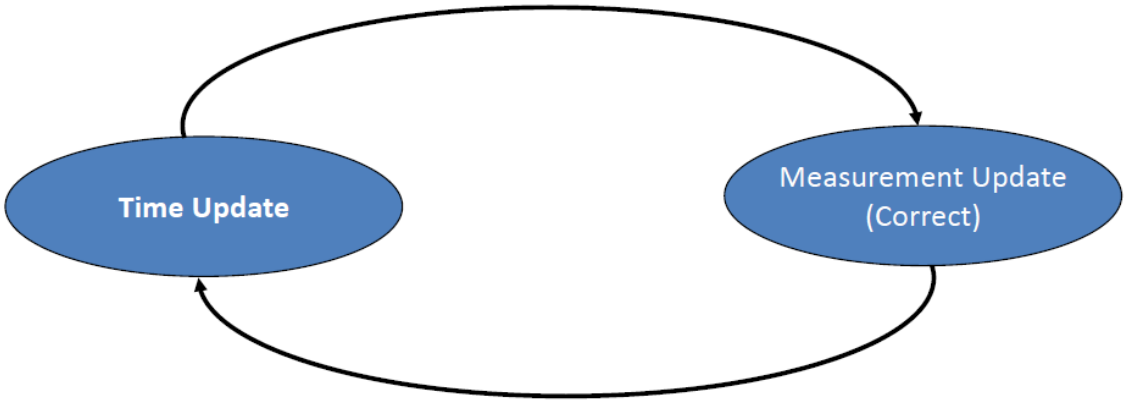

Figure 4.2 Prediction and correction process of KF

Assuming the following linear dynamic system:

$$x(k+1) = Ax(k) + Bu(k) + w(k) \tag{4-1}$$

$$z(k+1) = Cx(k+1) + v(k+1) \tag{4-2}$$

x is the state which needs to be estimated and u is the input. A, B and C are the system matrixes. z is the output vector which can be measured. w and v are zero mean, white Gaussian. The overall equations of KF are shown in Table 4.1. It is written in state-space representation.

Table 4.1 The equations of KF

Prediction (Time update)	Correction (Measurement update)
(1) Project the states ahead (a-priori) $\hat{x}_{k+1\|k} = A\hat{x}_{k\|k} + Bu_k$	**(1) Compute the Kalman gain** $K_{k+1} = P_{k+1\|k}C^T(CP_{k+1\|k}C^T + R_{k+1})^{-1}$
(2) Project the error covariance ahead $P_{k+1\|k} = AP_{k\|k}A^T + Q_k$	**(2) Update the estimation with the measurement (A posteriori estimation)** $\hat{x}_{k+1\|k+1} = \hat{x}_{k+1\|k} + K_{k+1}(z_{k+1} - C\hat{x}_{k+1\|k})$
	(3) Update the error covariance $P_{k+1\|k+1} = (1 - K_{k+1}C)P_{k+1\|k}$

However, for Li-ion battery, the dynamic model is not linear anymore. Therefore, some modification of KF needs to be made. EKF is an extended form of KF and used for the non-linear system [35]. In EKF, the system model is linearized around the current a priori state estimate and the linearized model is then used for calculating the Kalman gain to correct the predicted result. Let matrix C be the Jacobian of h with respect to x:

$$C_{ij} = \frac{\partial h_i}{\partial x_j}(x_k) \tag{4-3}$$

Then the KF equations can be rewritten as Table 4.2.

Table 4.2 The equations of EKF

Prediction (Time update)	Correction (Measurement update)
(1) Project the states ahead (a-priori) $\hat{x}_{k+1\|k} = A\hat{x}_{k\|k} + Bu_k$	**(1) Compute the Kalman gain** $K_{k+1} = P_{k+1\|k}C^T(CP_{k+1\|k}C^T + R_{k+1})^{-1}$
(2) Project the error covariance ahead $P_{k+1\|k} = AP_{k\|k}A^T + Q_k$	**(2) Update the estimation with the measurement (A posteriori estimation)** $\hat{x}_{k+1\|k+1} = \hat{x}_{k+1\|k} + K_{k+1}(z_{k+1} - h(\hat{x}_{k+1\|k}))$
	(3) Update the error covariance $P_{k+1\|k+1} = (1 - K_{k+1}C)P_{k+1\|k}$

However, EKF is not optimal for the nonlinear system and it may become unstable because of the linearization process in the presence of uncertainty. Therefore, a more robust filter [60], namely Smooth Variable Structure Filter will be introduced in the next section.

4.2 Smooth Variable Structure Filter

Smooth Variable Structure Filter was proposed by Habibi in 2007. SVSF uses the same concept as sliding mode control's switching action to correct state estimates and has been demonstrated robustness to modeling uncertainties and sensor noise [40]. It can be

applied to linear or non-linear systems and for both state and parameter estimation applications. It works by using the SVSF gain that forces the states to switch back and forth across the state trajectory within a region referred to as the existence subspace which is a function of modeling uncertainties.

Given the following nonlinear system:

$$\hat{x}_{k+1|k} = \hat{f}(x_{k|k}, u_k) \tag{4-4}$$

SVSF assumes the output equation is linear such that:

$$z_k = C\hat{x}_{k+1|k} + v_k \tag{4-5}$$

The estimation concept is shown in Figure 4.3. The SVSF gain is based on several parameters such as the a priori estimation errors, the a posteriori measurement errors, a smooth boundary layer widths ψ, a convergence rate γ, and an estimate measurement matrix. The overall SVSF equations are shown in Table 4.3.

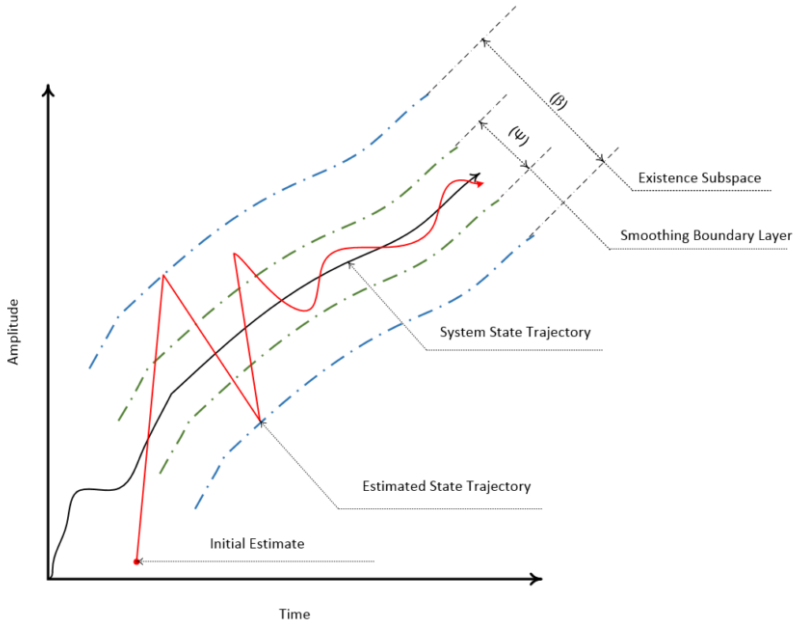

Figure 4.3 SVSF estimation concept

Table 4.3 The equations of SVSF

Prediction (Time update)	Correction (Measurement update)
(1) Project the states ahead (a-priori) $\hat{x}_{k+1\|k} = f(\hat{x}_{k\|k}, u_k)$	**(1) Compute the SVSF gain** $K_{k+1} = \hat{C}^{-1}(\lvert e_{z,k+1\|k} \rvert + \gamma \lvert e_{z,k\|k} \rvert) \circ sat(\frac{e_{z,k+1\|k}}{\psi})$
(2) Project a priori estimation error $e_{z,k+1\|k} = z_{k+1} - \hat{z}_{k+1\|k}$	**(2) Update the a posteriori state estimation** $\hat{x}_{k+1\|k+1} = \hat{x}_{k+1\|k} + K_{k+1}$
	(3) Update the a posteriori estimation error $e_{z,k+1\|k+1} = z_{k+1} - \hat{z}_{k+1\|k+1}$

The smoothing function can help to filter out the chattering with a known boundary layer ψ by defining

$$sat(\frac{e_{z,k+1|k}}{\psi}) = \begin{cases} \frac{e_{z,k+1|k}}{\psi} & \left|\frac{e_{z,k+1|k}}{\psi}\right| \leq 1 \\ sign(\frac{e_{z,k+1|k}}{\psi}) & \left|\frac{e_{z,k+1|k}}{\psi}\right| > 1 \end{cases} \tag{4-6}$$

Outside of the boundary layer, the sign function is maintained to ensure stability while inside of the layer, the SVSF gain is interpolated to obtain a smooth function.

The proof of stability of SVSF is discussed in [61]. According to [40], the SVSF estimation process is stable and will converge to the existence subspace during the reachability phase according to equation

$$\left|e_{z,k+1|k+1}\right| < \left|e_{z,k|k}\right| \tag{4-7}$$

4.3 Estimation Results

The estimation results based on optimized battery combined model for both EKF and SVSF under white Gaussian noise are presented in this section. After trial and error, the system and measurement noise covariance in EKF, and the convergence rate and boundary layers in SVSF were obtained as in Table 4.4.

Table 4.4 The EKF System and Measurement Noise Covariance, and the SVSF Convergence Rate and Boundary Layers

Filter Parameters	EKF	SVSF
Q	1e-10	/
R	0.1	/
ψ	/	3
γ	/	0.8

The estimated SOC is initialized at 0.7, while the actual SOC is at 0.9. The SOC estimation results both for fresh cell and aged cell by EKF and SVSF are shown in Figure 4.4 and Figure 4.5. Figure 4.6 shows the zoom-in configuration at the very beginning of the estimation process. Furthermore, the Root Mean Square Error (RMSE) associated with SOC estimation compared to the actual value is shown in Table 4.5, respectively.

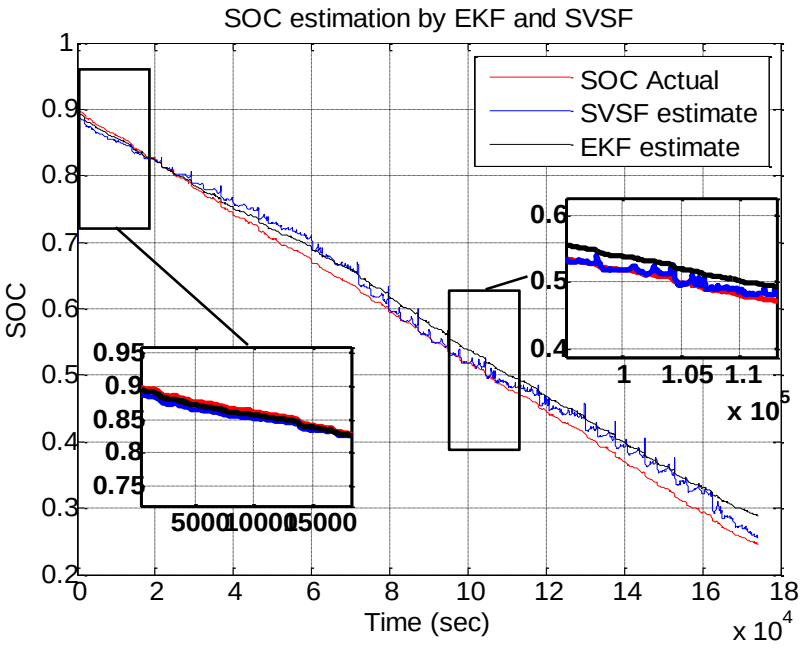

Figure 4.4 Estimated Vs. Actual SOC by EKF and SVSF estimation strategies (Fresh cell)

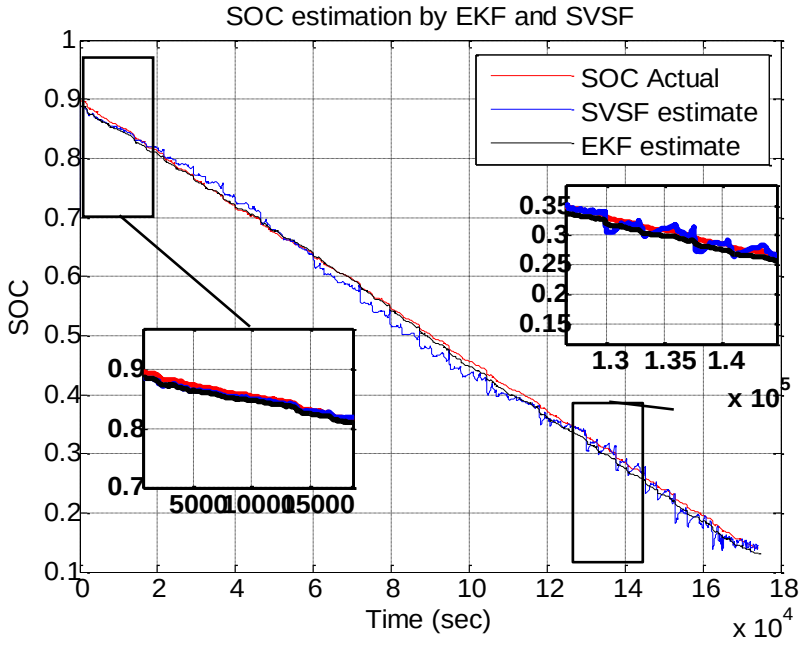

Figure 4.5 Estimated Vs. Actual SOC by EKF and SVSF estimation strategies (Aged cell)

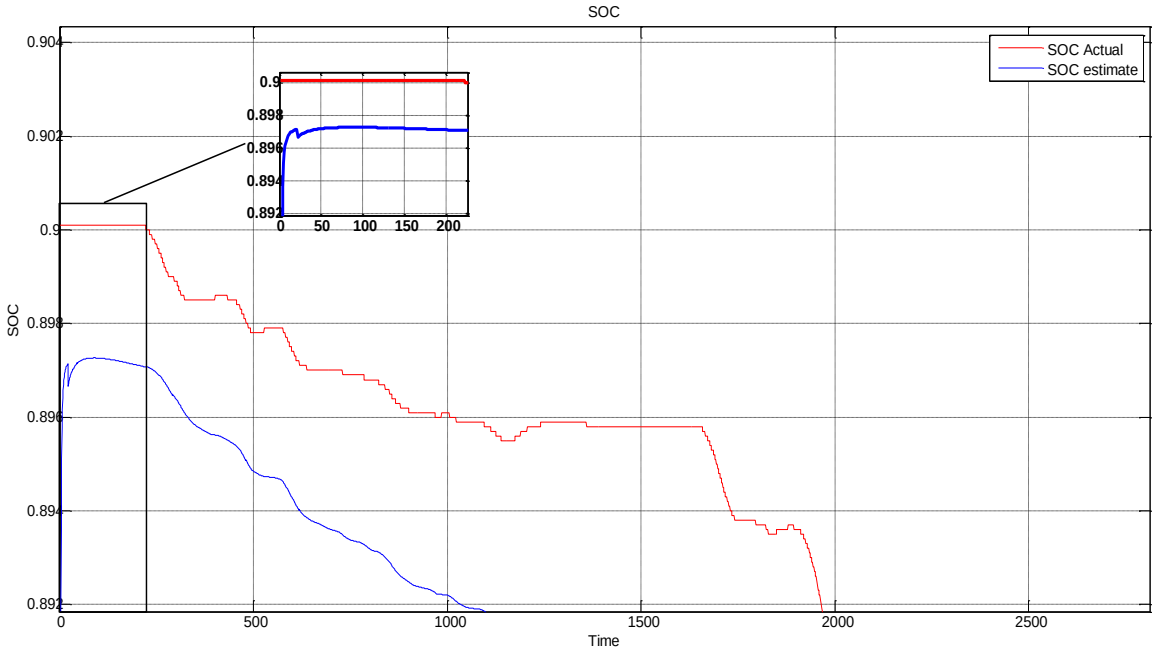

Figure 4.6 Zoom-in at the very beginning of estimation process

Table 4.5 Estimation Error

RMSE	SOC error for fresh cell	SOC error for aged cell
EKF	2.26%	0.75%
SVSF	1.68%	1.30%

The result demonstrates that both EKF and SVSF provide fast convergence under white Gaussian noise even though the error between the initial SOC and the actual SOC is quite different. Moreover, EKF and SVSF can provide an excellent estimation accuracy if the filter parameters are properly tuned. Specifically, when the model is relatively accurate, such as aged cell model, EKF shows better results compared to SVSF. However, as discussed in chapter 3, the battery aged model is more accurate than fresh model. As the

model uncertainties grow, SVSF can provide a better estimation result, which shows a better robustness of SVSF compared to EKF.

Chapter 5 : Cell Balancing Physical Implementation

5.1 “Fly-Back” Converter

“Fly-back” converter topology is widely used for output powers from about 150 down to under 5 W. Its great initial attraction is that it has no secondary output inductors compared with some other topologies. The consequent savings in cost and volume of the output inductors is a significant advantage [62].

Most topologies used in balancer today employ a unidirectional (discharge only) approach. The simplest of these operate by switching in a resistor across the highest voltage cell(s) in the stack (passive balancing). No charge is recovered in this approach, instead it is dissipated as heat in the resistive element. This can be improved by employing an energy storage element (inductive or capacitive) to transfer charge from the highest voltage cell(s) in the stack to other lower voltage cells in the stack (active balancing). This can be very efficient (in terms of charge recovery) for the case where only a few cells in the overall stack are high, but will be very inefficient (and time consuming) for the case where only a few cells in the overall stack are low. A bi-directional active balancing approach, such as employed by the “Fly-back” topology, shown in Figure 5.1, is needed to achieve minimum balancing time and maximum charge recovery for all common cell capacity errors [63].

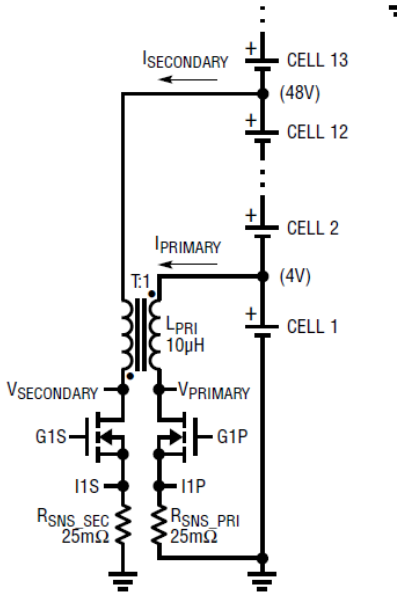

Figure 5.1 “Fly-back” topology [63]

The transformer in this topology no longer works in the function of a transformer but as an inductor. “Fly-back” operation can be easily recognized from the dots on the transformer primary and secondary. When dots locates on the opposite side, it is “Fly-back”. Otherwise, it’s called “Fly-forward”. “Fly-back” converter can work both in discharging and charging mode. When discharging, in the beginning, the primary MOSFET gate G1P opens. During the on time, the individual cell discharges, and there is a fixed voltage and current in primary ramps up linearly. At the end of the on time, the primary current reaches a limit and represents a stored energy of

$$E = \frac{L_p (I_p)^2}{2} \tag{5-1}$$

Where L_p is the primary magnetizing inductance and I_p is the primary maximum current. Now when G1P turns off, the current can be transferred to secondary at an amplitude

$$I_s = I_p(N_p / N_s) \tag{5-2}$$

Where N_p and N_s are the turn number of primary and secondary. Then the secondary current flows out to the stack and ramps down to zero linearly. The discharging waveform is shown in Figure 5.2. The charging process works similarly as discharging.

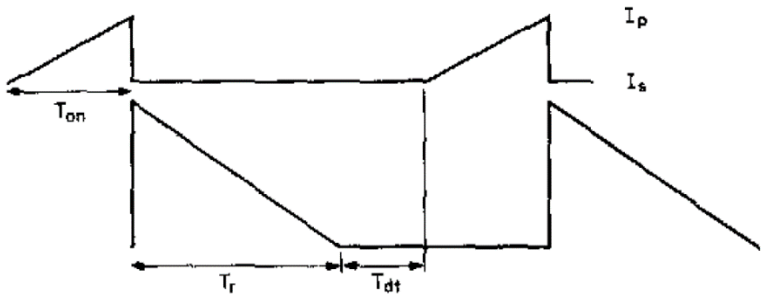

Figure 5.2 Current waveform of "Fly-back" converter [62]

5.2 Hardware Design

5.2.1 Balancer Design

The architecture of balancer is bi-directional synchronous "Fly-back" and designed based on LTC3300-1. Each LTC3300-1 can balance up to 6 series connected batteries with an input common mode voltage up to 36V and contains six independent synchronous "Fly-back" controllers that are capable of directly charging or discharging an individual cell. Balancing current is scalable with external components. Each balancer operates

independently of the others and provides a means for bidirectional charge transfer between an individual cell and a larger group cells. A unique level-shifting SPI-compatible serial interface enables multiple LTC3300-1 devices to be connected in series without isolators, allowing for balancing of every cell in a long string of series-connected batteries. Fault protection features include read back capability, Cyclic Redundancy Check (CRC) error detection, maximum on-time volt-second clamps, and overvoltage shutoffs.

LTC3300-1 provides a 50 mV reference voltage to calculate the programmed charging or discharge peak current based on the following equation:

$$I_{peak\_pri} = \frac{50mV}{R_{pri}} \tag{5-3}$$

$$I_{peak\_sec} = \frac{50mV}{R_{sec}} \tag{5-4}$$

Where I_{peak_pri} and R_{pri} are the primary peak current and sense resistance; I_{peak_sec} and R_{sec} are the secondary peak current and sense resistance. Each balancer's charge transfer frequency and duty cycle depend on many factors including I_{peak_pri}, I_{peak_sec}, the number of secondary-side cells S, the transformer turns ratio T, transformer winding inductance L and the cell voltage $V_{\_cell}$. The frequency of switching seen at the gate of driver output is given by

$$f_{discharge} = \frac{S}{S+T} \bullet \frac{V_{cell}}{L \bullet I_{peak\_pri}} \tag{5-5}$$

$$f_{charge} = \frac{S}{S+T} \bullet \frac{V_{cell}}{L \bullet I_{peak\_sec} \bullet T} \tag{5-6}$$

LTC3300-1 contains programmable fault protection clamps which limit the amount of time that current is allowed to ramp in either the primary or secondary windings in the event of a shorted sense resistor. Maximum on time for all primary connections (active during cell discharging) and all secondary connections (active during cell charging) is individually programmable by connecting resistors from the R_{tonp} and R_{tons} to V^- according to the following equations

$$t_{on\max\_pri} = 7.2\mu s \bullet \frac{R_{tonp}}{20k\Omega} \tag{5-7}$$

$$t_{on\max\_sec} = 1.2\mu s \bullet \frac{R_{tons}}{15k\Omega} \tag{5-8}$$

Another protection in LTC3300-1 is over-temperature protection which can shut down all active balancing if the inner silicon temperature rises to approximately 155 ℃. As shown in Figure 5.3, the maximum temperature of balancer board is around 51.3 ℃ after one-hour operation and the point is located at MOSFET. So both the LTC3300-1 and the other components can normally work without overheating.

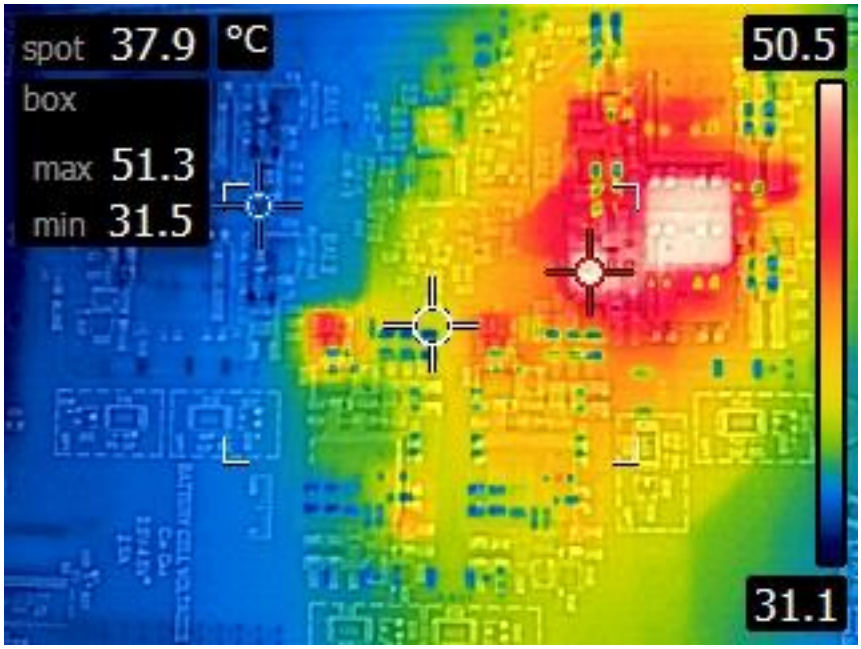

Figure 5.3 Thermal chart of balancer board

In order to handle the peak balancing current, external transistors for both primary and secondary windings must be chosen to have a safety drain to source breakdown voltage. In addition, considering leakage inductance ringing, good design practice recommends increasing breakdown voltage rating by at least 20%. SiR882DP/N MOSFET with 60A/25A and 100V maximum drain to source current and voltage are tested in the experiment and successfully drive the circuit with safety breakdown voltage.

Another significant component on balancer board is transformer. A 1:2 turns ratio (primary to secondary) with 3.5μH inductance transformer is used in the balance application. The primary is directly connected to the individual cell and the secondary is connected to the stack. If a large number of cells in the secondary stack is desired for more efficient balancing, a transformer with higher turns ratio can be selected. In this case, the

external MOSFET needs to be rated for a higher voltage. What's more, under all these circumstances, the saturation current of the transformer must be selected to be higher than the peak current.

Furthermore, in the transient process, the peak drain ringing voltage seen at primary and secondary MOSFETs is quite large and very easy to break the components. Therefore, in order to keep the MOSFETs in the safe working area, a series connected resistor and capacitor snubber network in parallel with each transformer winding is placed in PCB. The value of R and C are determined by trial and error.

The balancing current for four series connected Li-ion batteries seen at sense resistor is shown in Figure 5.4 and Figure 5.5.

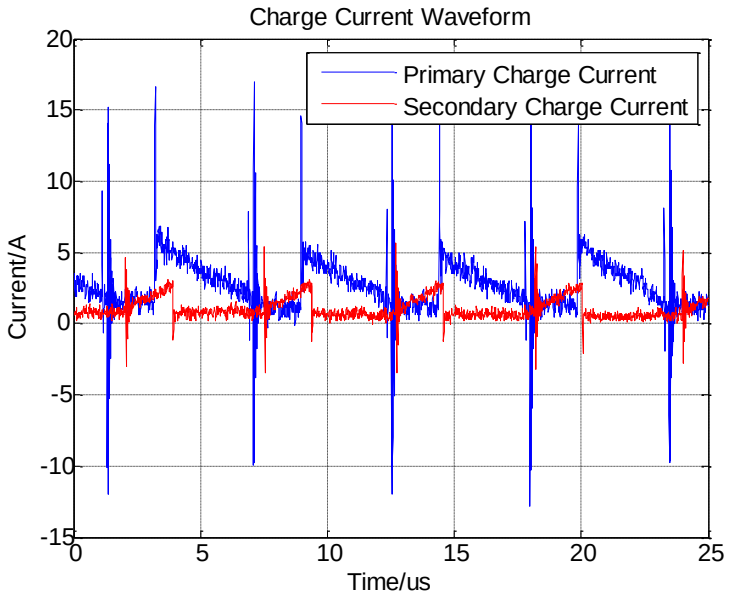

Figure 5.4 Charge current waveform

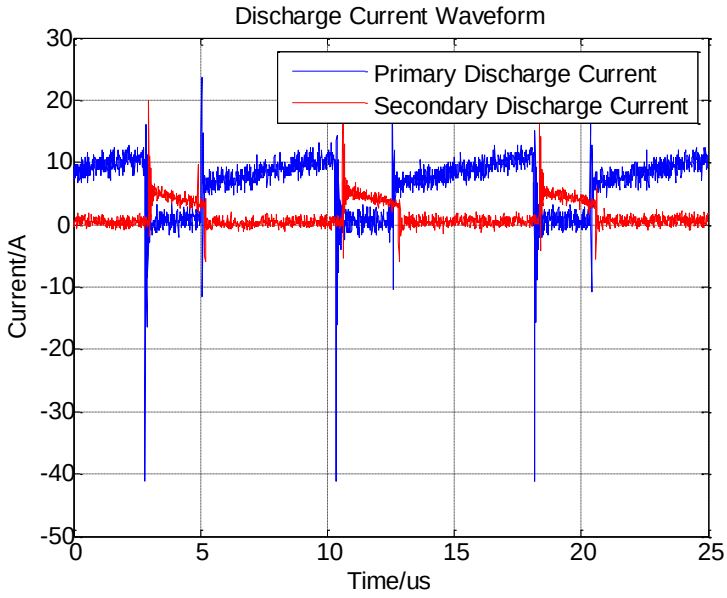

Figure 5.5 Discharge current waveform

The designed “Fly-back” topology works in discontinuous mode when charging and continuous mode when discharging in order to improve the mean value of balancing current. The overall physical parameters are shown in Table 5.1, and measurement parameters are shown in Table 5.2

Table 5.1 Physical Parameters

Physical Parameter	Symbol	Value	Unit
The number of cells	S	4	
Turns ratio (primary to secondary)	T	1:2	
Transformer inductance	L	3.5	μH
Sense resistor (primary)	R_{pri}	0.005	Ω
Sense resistor (secondary)	R_{sec}	0.010	Ω
Snubber resistor	R	20	Ω
Snubber capacitor	C	470	pF

Table 5.2 Measurement Parameters

Measurement Parameter	Symbol	Value	Unit
Peak current (primary, discharge)	$I_{peak\_pri\_d}$	10	A
Peak current (secondary, discharge)	$I_{peak\_sec\_d}$	5	A
Peak current (primary, charge)	$I_{peak\_pri\_c}$	5	A
Peak current (secondary, charge)	$I_{peak\_sec\_c}$	2.5	A
Mean current (primary, discharge)	$I_{mean\_pri\_d}$	5.33	A
Mean current (secondary, discharge)	$I_{mean\_sec\_d}$	1.07	A
Mean current (primary, charge)	$I_{mean\_pri\_c}$	1.43	A
Mean current (secondary, charge)	$I_{mean\_sec\_c}$	0.38	A
Switching frequency (charge)	f_{charge}	175.4	kHz
Switching frequency (discharge)	$f_{discharge}$	133.5	kHz
Maximum on time (primary)	t_{onmax_pri}	11.95	μs
Maximum on time (secondary)	t_{onmax_sec}	1.89	μs

5.2.2 Controller Design

The controller is developed based on XMC4500 microcontroller for industrial applications. It is the member of XMC4000 family based on the ARM Cortex-M4 32-bit processor core. The XMC4000 is a family of high performance and energy efficient microcontrollers optimized for industrial connectivity, industrial control, power conversion, sensing and control. The system block diagram is shown in Figure 5.6.

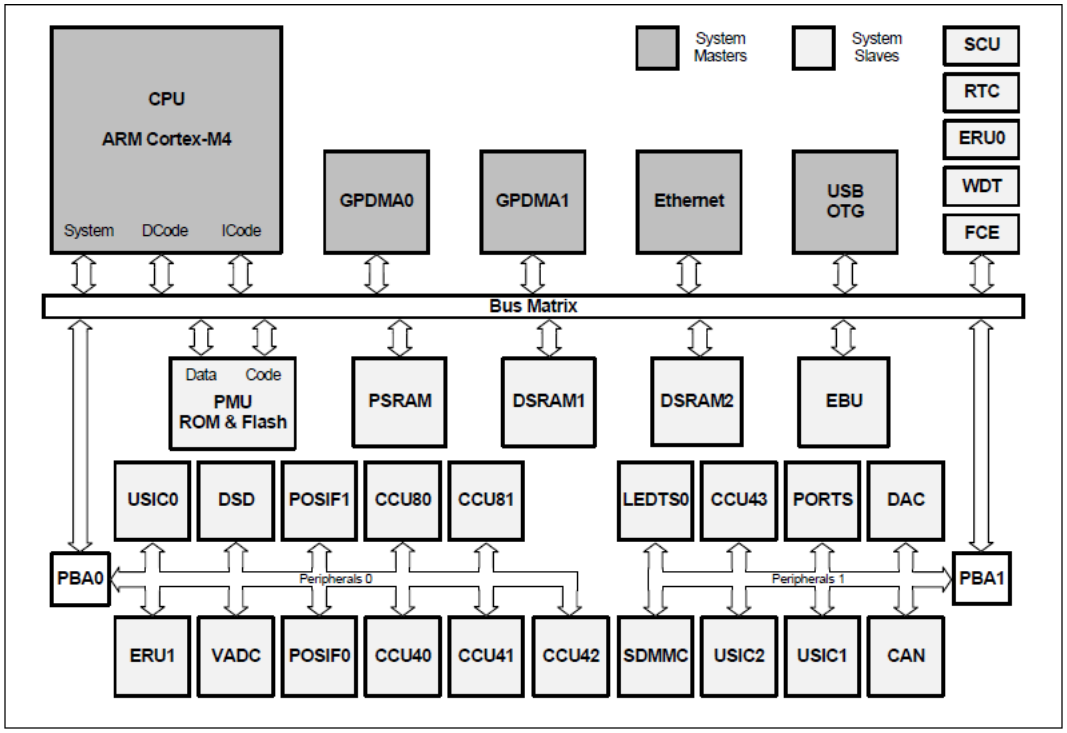

Figure 5.6 XMC4500 system block diagram

The features of XMC4500 in balancing application include analog and digital input, hibernate and real-time clock, USB communication, Controller Area Network (CAN) interface, six Universal Serial Interface Channels (USIC) usable as UART, SPI, I2C etc., Direct Memory Access (DMA) with up to 12 channels. The designed PCBs of balancer and controller are shown in Figure 5.7.

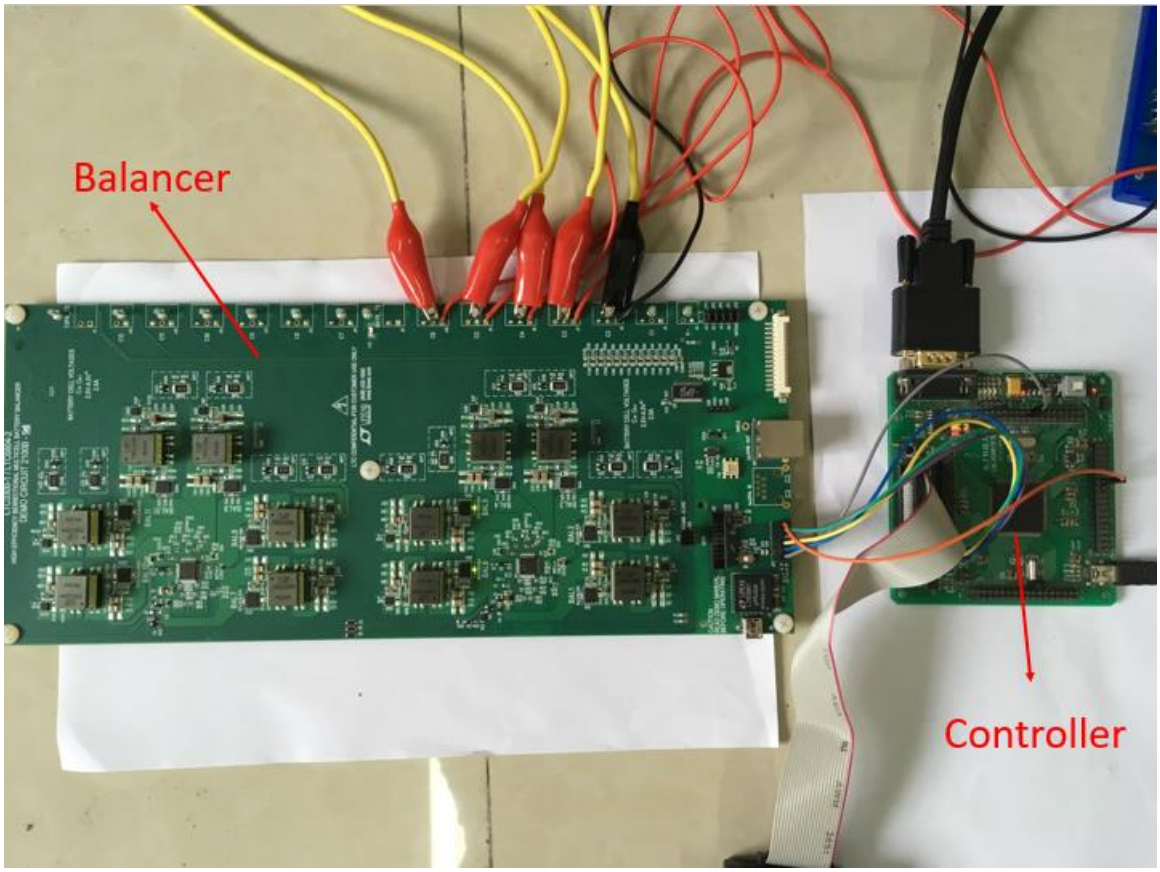

Figure 5.7 Balancer and controller

5.3 Experiment Configuration

5.3.1 Data Collection

The experimental data such as cell voltage are collected by a multi-cell battery monitor LTC6804. It is a 3rd generation high accurate and fast battery monitor that measures up to 12 series connected battery cells with a total measurement error of less than 1.2mV. The cell measurement range of 0V to 5V makes the LTC6804 suitable for most battery chemistries. All 12 cell voltages can be captured in 290μs, and lower data acquisition rates can be selected for high noise reduction. The cell voltage information is

sampling by LTC6804 from an existing PCB of BMS (Figure 5.8) and then can be transmitted to controller.

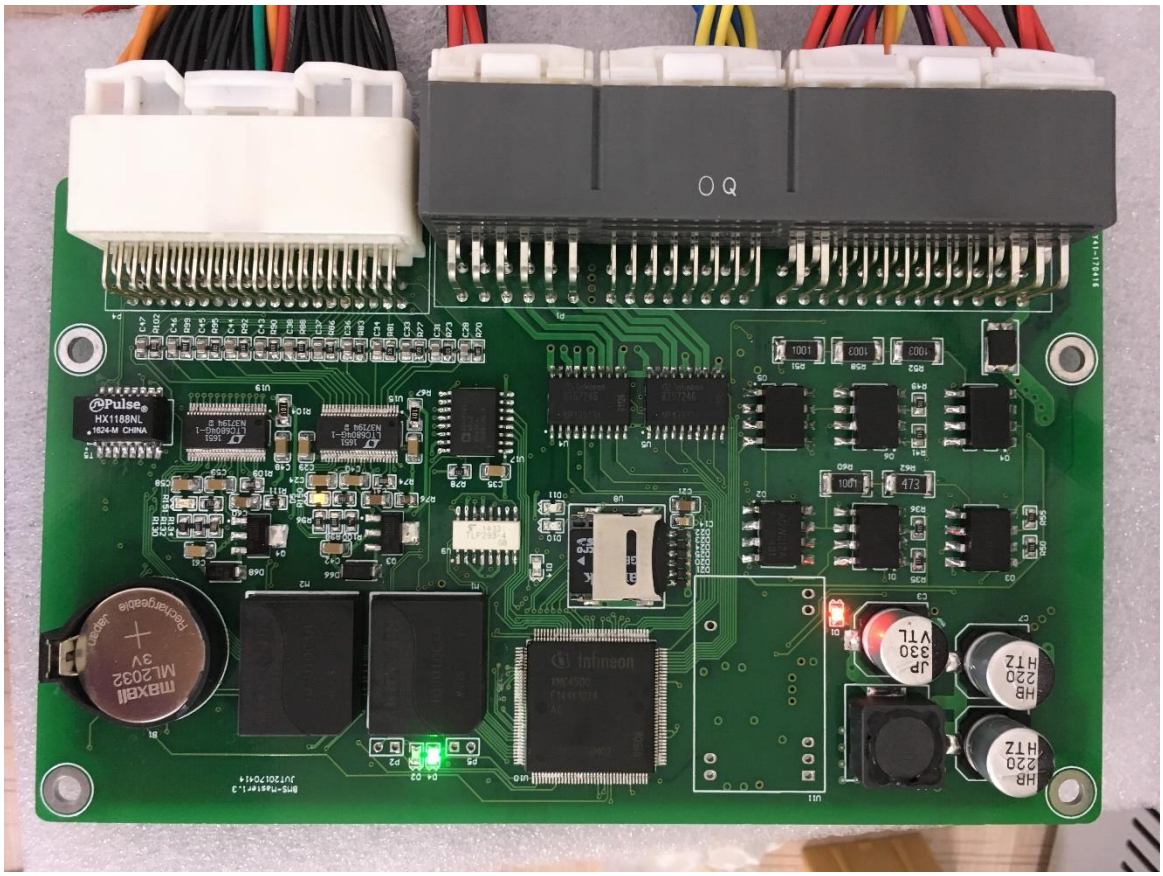

Figure 5.8 Battery management system

The battery pack current and voltage can be captured by Repower High-power Battery Testing System CDS-200V80A which is shown in Figure 5.9. It is not only a data recording devices but also a test system which can charge and discharge the battery pack in Constant-Current Constant-Voltage (CCCV) mode, constant power mode and driving cycle mode with 0.1% voltage and current precision.

Figure 5.9 Repower High-power Battery System CDS-200V80A

5.3.2 Communication

Due to different communication interface for the different devices, several communication protocols are used for information interaction. The overall communication structure is shown in Figure 5.10.

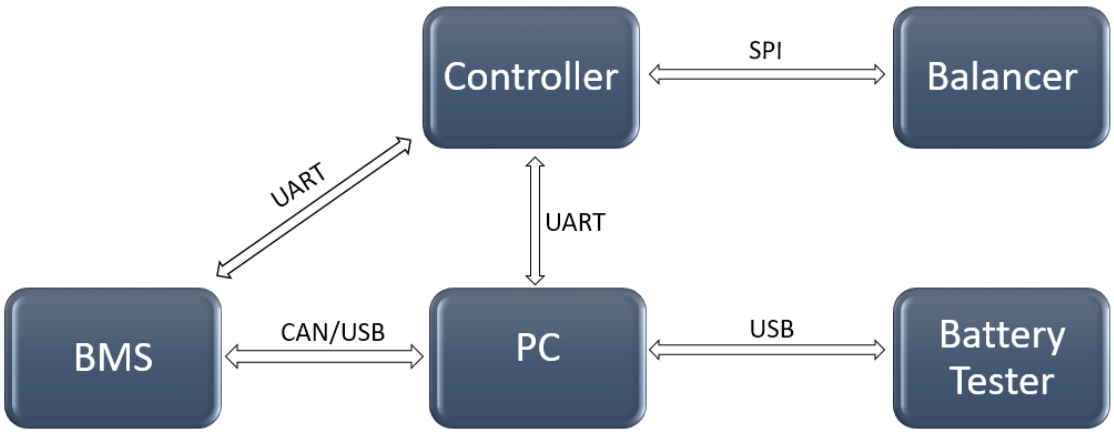

Figure 5.10 Overall communication structure

The Battery tester transmits pack current and voltage through USB to PC to show the current pack status; the BMS takes responsibility of sampling the cell voltage and pack current with the help of LTC6804 and transmits to PC and controller; the controller receives pack current, pack voltage and cell voltage from BMS through UART in order to calculate SOC, and then sends SOC information to PC via UART and balancer command to balancer based on balancing algorithm via SPI; the PC collects all information from the other devices for the purpose of monitoring by the user. Figure 5.11 shows part of the experiment configuration.

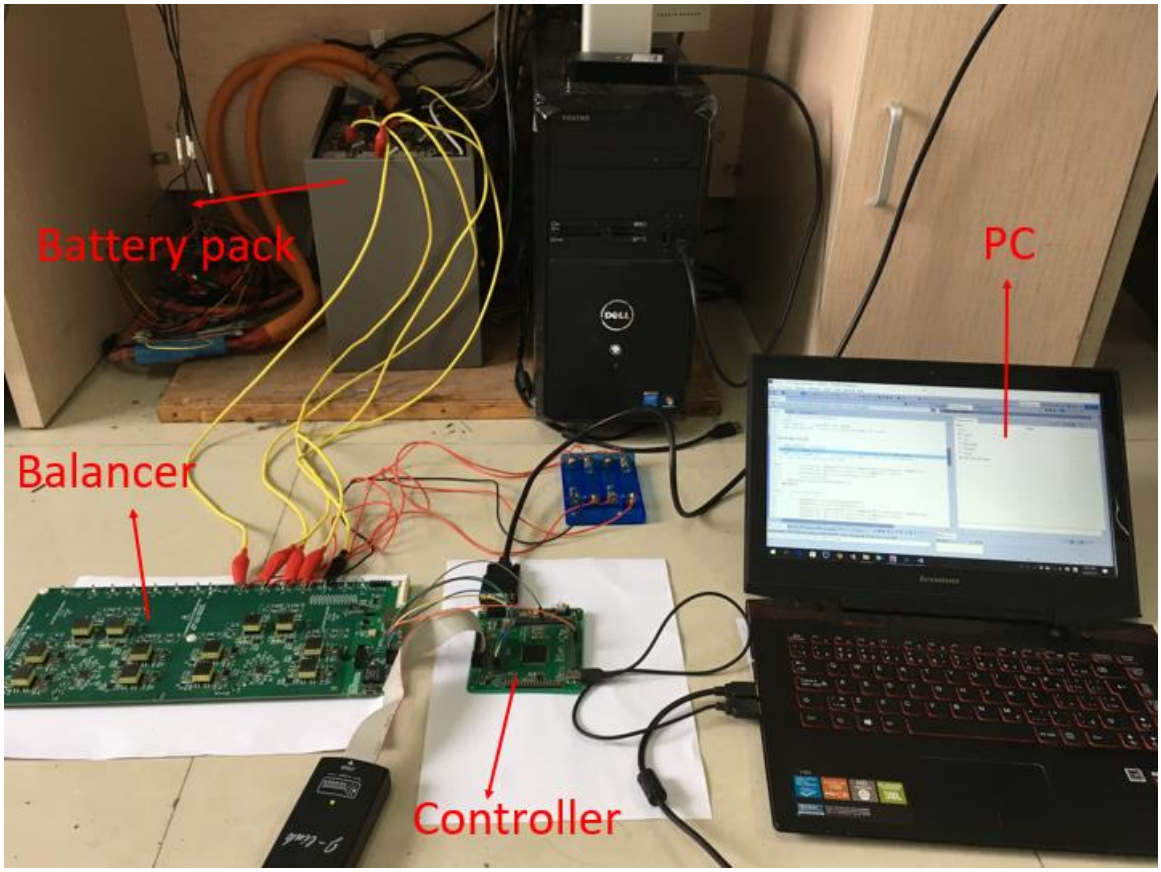

Figure 5.11 Part of experiment configuration

5.3.3 Balancing Algorithm

The balancing algorithm is coded in DAVE 4.2.6 development platform based on C. It is free of charge Eclipse based Integrated Development Environment (IDE) using C-compiler providing extensive, configurable, and reusable code repository for XMC industrial microcontroller powered by ARM Cortex-M processors. What's more, DAVE is an application oriented code repository merged with graphical system design methods, Graphical User Interface (GUI) based configuration and automatic code generator to guide XMC microcontroller user along the entire process from Evaluation-to-Production (E2P).

XMC library and DAVE generated code can be used with other 3rd party tool chains. The XMC library can be seen in Figure 5.12 and it can be simply dragged to IDE and configured in GUI, so that it saves an amount of time wasting in configuring registers.

System:	Timer/PWM:	Analog-mixed Signal:	Communication:	Application specific:	Examples:
• DMA • ERU • FCE • FLASH • GPIO • MATH • PAU • PRNG • RTC • SCU • WDT	• CCU4 • CCU8 • HRPWM • POSIF	• ACMP • ADC • DAC • DSD	• CAN • I2C • I2S • SPI • UART • USB • USIC • Ethernet • EtherCAT ®	• BCCU • LEDTS • MATH • POSIF • HRPWM	• Examples for all peripherhals drivers and ARM, GCC, IAR, and Tasking compiler • Project files for ARM/KEIL MDK • Project files for IAR System Embedded Workbench

Figure 5.12 XMC library

At the beginning of balancing, the controller receives the initial SOC information from BMS based on the experimental OCV-SOC data which can be seen in Figure 5.13. And then starts to calculate SOC based on Coulomb counting.

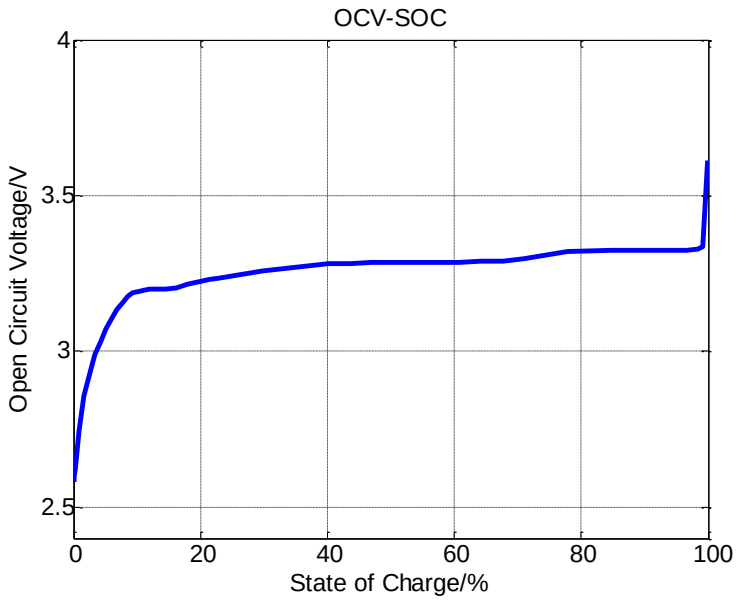

Figure 5.13 OCV Vs SOC

The balancing algorithm is based on the calculated mean SOC in the controller as

$$\overline{SOC} = \sum_{c=1}^{N} \frac{SOC_c(t)}{N} \tag{5-9}$$

Where N is the number of cells, $SOC_c(t)$ is the cell SOC at the current time. Every time the controller receives all data from other devices and then calculate the current SOC for every individual cell. If the SOC of a particular cell is lower than mean SOC, the controller will send a charge command to the balancer to charge the specific cell. Otherwise, it will send discharge command to balancer. However, in the real application, the mean value of SOC is affected by the battery pack, so the SOC of individual cell cannot keep the same value as mean SOC over entire cycle. Another issue is that sometimes it will overbalance the cell due to the constant balancing current. Overbalancing can result in voltage chattering problem and reduce the efficiency. Therefore, a threshold of SOC difference value between

individual SOC and mean SOC needs to be set to avoid chattering and improve balancing efficiency. A large threshold value will lead to large SOC difference and underbalance the cell. On the other hand, a small threshold value cannot be gotten an effective performance. After trial and error, an acceptable result can be obtained by setting the SOC threshold to 0.03%. If the SOC of the individual cell is within the threshold, no balancing action will apply.

The programming logic flow diagram is shown in Figure 5.14.

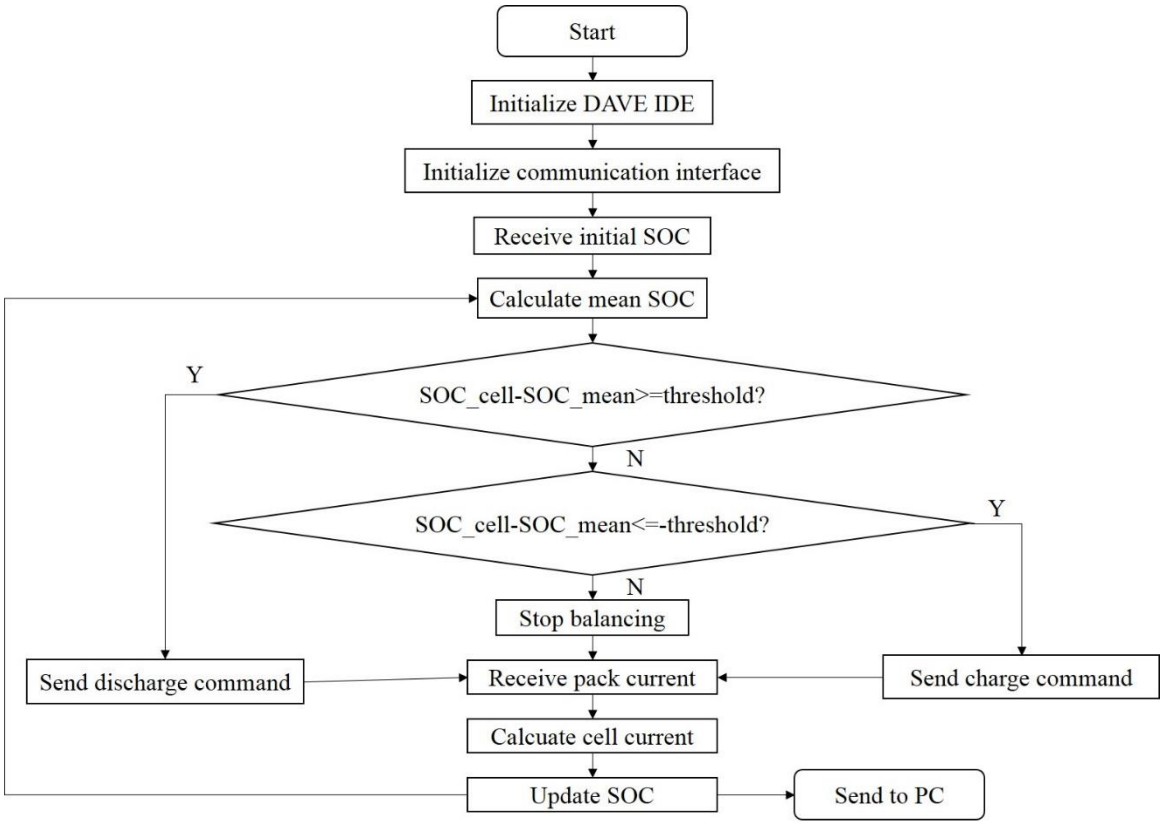

Figure 5.14 Programming logic flow diagram

5.4 Experimental Results

The above design and algorithm are applied to four 55Ah series connected Li-ion batteries in discharging mode, idle mode and plug-in charging mode to test the balancing performance based on both SOC and OCV, and compare with the previous test for transformer and capacitor which can balance battery voltage about 10mV per hours. After every test cycle, the battery pack can relax for a while to get confidential OCV to check that when SOC is balanced, whether the corresponding voltage is balanced as well.

5.4.1 Balancing Performance in Discharging Mode

Dynamic Stress Tests (DST) for Li-ion battery are used to demonstrate whether the balancing system can work effectively in discharging mode. And DST cycle current can be seen in Figure 5.15. The initial SOC of four cells are 96.693%, 94.714%, 93.684%, and 89.622%, respectively. The experimental results in discharging mode are shown in Figure 5.16 and Figure 5.17.

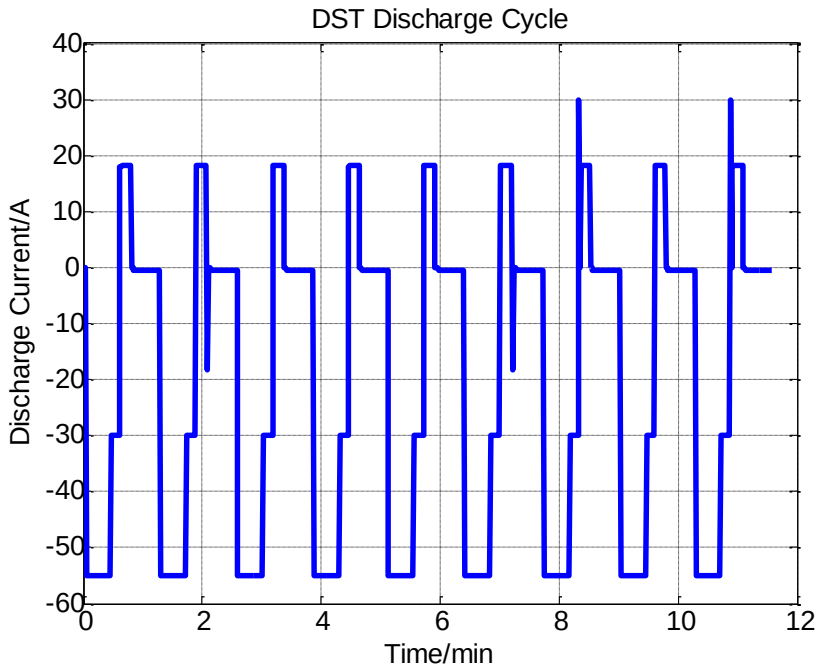

Figure 5.15 DST discharge cycle

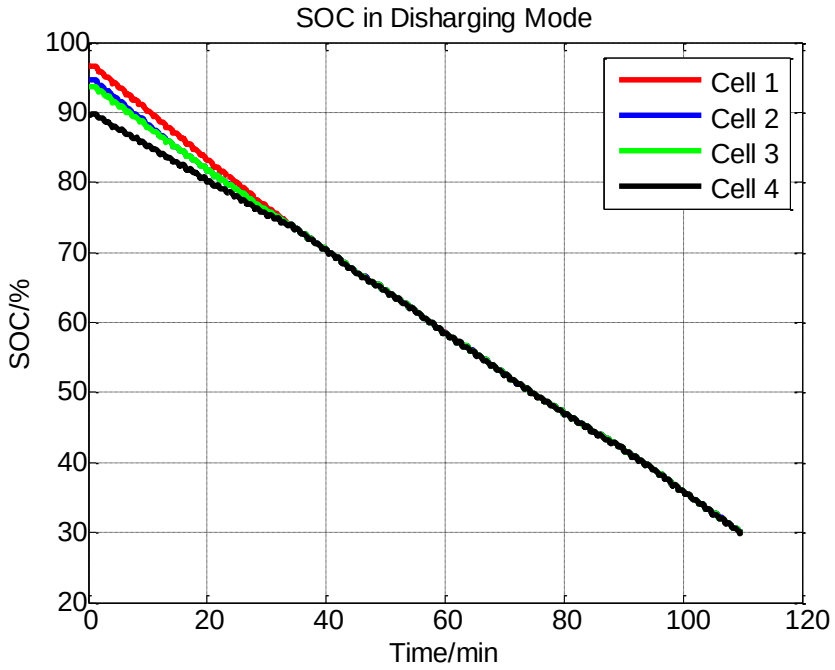

Figure 5.16 SOC in discharging mode

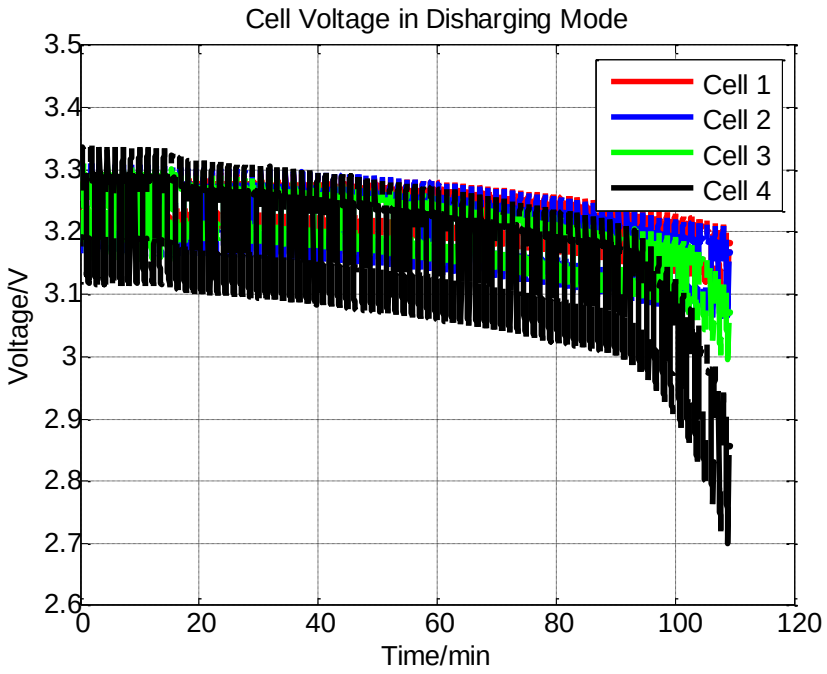

Figure 5.17 Cell voltage in discharging mode

From results of these two plots, “Fly-back” topology has very fast SOC balancing speed. It can balance 7% SOC difference in 30 minutes due to high balancing current. However, in the cell voltage diagram, the voltage of cell 4 drops very quickly in the end and diverges with the others. At this time, the SOC and voltage are uncoordinated. The main reason for this problem is that considering Figure 5.13, in the very beginning, the initial SOC is around 90% where it has already located in the flat area in OCV-SOC curve. Therefore, several SOC values correspond only one OCV and then OCV-SOC mismatch happens. Furthermore, it is tough to charge a battery over 90% SOC to cross the flat area to reach ascending section due to some battery inner chemistry characteristics. So the initial SOC captured in BMS is not accurate and results in the following error.

5.4.2 Balancing Performance in Idle Mode

When the vehicle is in the idle state, for instance, parking at night, it is a good chance for balancing system to rematch the battery pack after the all-day usage. The initial SOC values of four Li-ion batteries are 3.319%, 5.144%, 4.322%, and 6.994%, respectively. The balancing performance in idle mode is shown in Figure 5.18 and Figure 5.19.

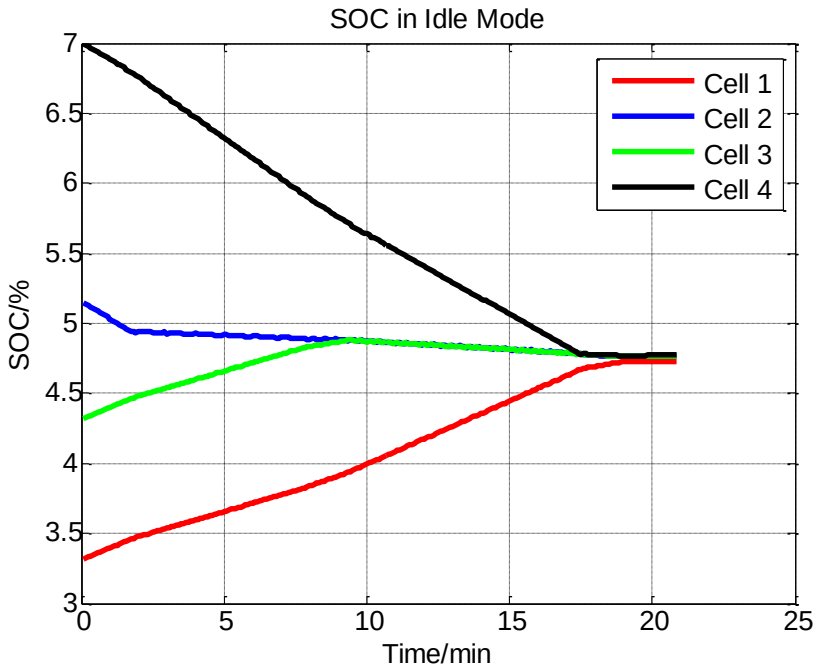

Figure 5.18 SOC in idle mode

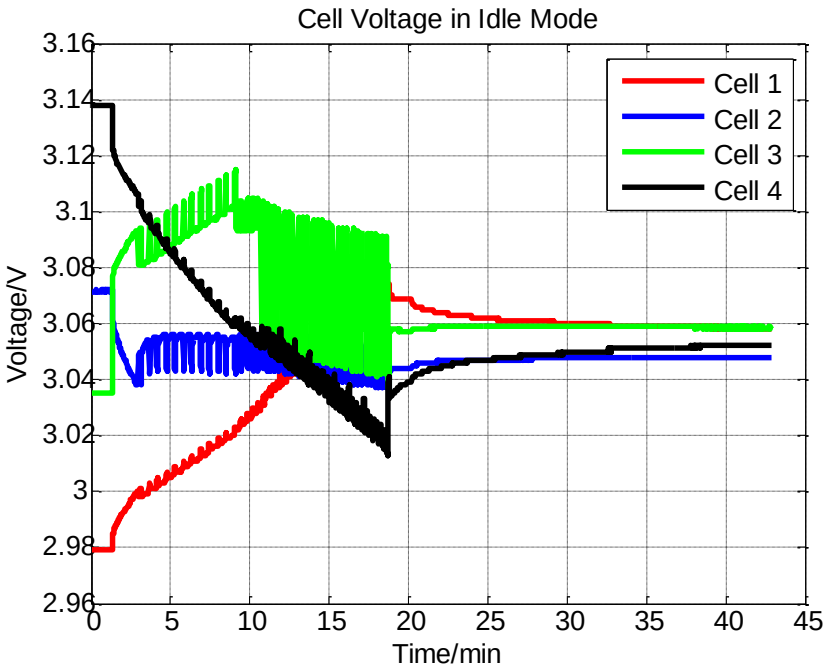

Figure 5.19 Cell voltage in idle mode

As seen in the above figures, the "Fly-back" topology can work in bi-directional mode (charging and discharging) and quickly balance almost 4% SOC difference only in around 17 minutes. The previous and post SOC and cell voltage differences are shown in Table 5.3. It shows both SOC and cell voltage can be balanced correspondingly.

Table 5.3 SOC and Voltage Difference Before and After Balancing

	SOC difference	Cell voltage difference
Previous	3.6750	159mV
Post	0.0420	10mV

5.4.3 Balancing Performance in Plug-in Charging Mode

A standard battery charging protocol known as Constant-current Constant-voltage is used for charging Li-ion battery which can be vulnerable to damage if the upper voltage limit is exceeded. The initial SOC values of four cells are 9.004%, 5.254%, 16.718%, and 6.092%, respectively. The experimental results are shown in Figure 5.20 and Figure 5.21.

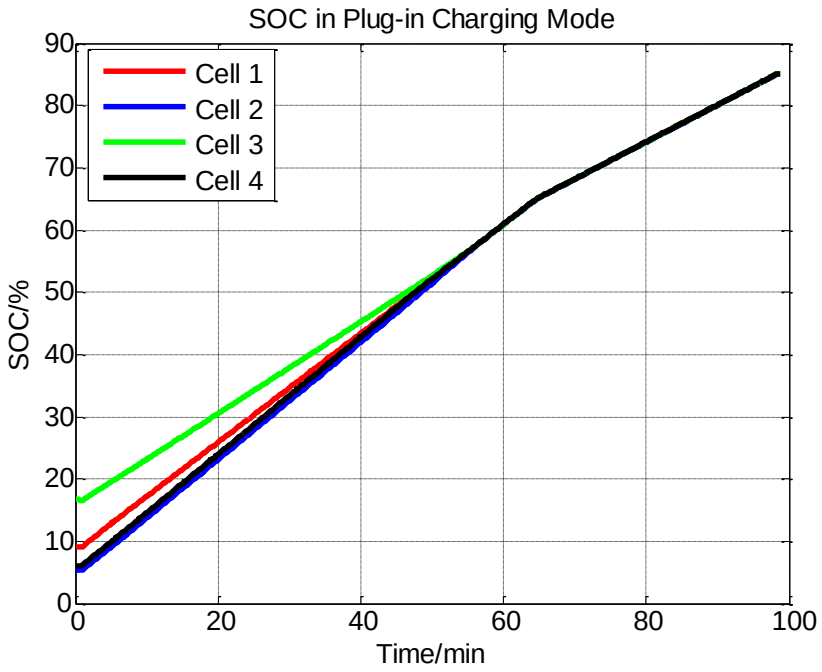

Figure 5.20 SOC in plug-in charging mode

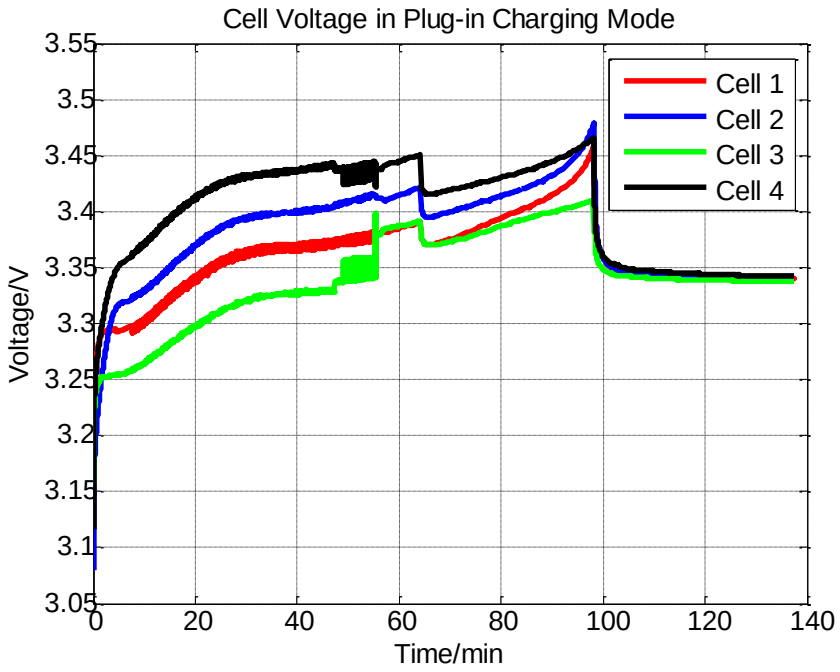

Figure 5.21 Cell voltage in plug-in charging mode

From the above figures, the charging balancing takes a little bit longer than discharging balancing and bi-directional balancing due to relatively smaller balancing current. It can balance 11% SOC difference in around one hour. But the final balancing performance is quite good. The previous and post SOC and cell voltage differences are shown in Table 5.4.

Table 5.4 SOC and Voltage Difference Before and After Balancing

	SOC difference	Cell voltage difference
Previous	11.4640	103mV
Post	0.0420	5mV

5.5 Summary

From the above experimental results, a summary can be drawn as follows: “Fly-back” topology can work in bi-directional mode. Compared with the other topologies, for instance, the resistor (passive balancing), transformer and capacitor, it can balance the entire battery pack effectively and quickly due to bi-direction and large balancing current. However, the balancing algorithm highly depends on battery SOC. So accurate SOC estimation is necessary for physical implementation. As shown in discharging mode, if the initial estimated SOC cannot be trusted, it will get a bad balancing performance: the cell voltage diverges remarkably. On the other hand, for idle and plug-in charging mode, since the initial SOC is quite accurate, the cell voltage can match SOC very well and it shows a quite good balancing result. In conclusion, in order to get relative accurate SOC estimation and good balancing performance, it recommends that the batteries can be balanced from or within the section of 0-10% SOC. In this area, the voltage and SOC can show the noticeable difference and are one to one correspondence. In a word, avoiding OCV-SOC flat area can improve the balancing performance.

Chapter 6 : Active Cell Balancing Optimization

While a great number of battery balancing circuit topologies are proposed, the unique control objective typically pursued is equalization of single cell charge. However, a balancing circuit could offer potentially more control features, especially with topologies able to provide bi-directional power flow control. In this chapter, an active SOC-based cell balancing optimization is implemented in MATLAB in order to optimize the battery capacity and thermal effect.

6.1 Cell Imbalance

Series cell SOC mismatches consist of tiny imperfections in construction that can result in soft shorts inside the cell, that can increase the self-discharge rate by up to 3%, per month, of the cell capacity [10]. They can also affect the charge acceptance of the cell. Most cells do not have soft shorts and can hold much of their capacity for years but some cells which otherwise meet specifications do not exhibit soft shorts until they leave the factory. When used in a single cell pack, a cell with soft shorts can be recharged and shows a little capacity loss. But, in a series pack, when one cell loses no capacity, while another cell loses 3% per month, the effect is a relatively continuous loss of pack capacity. Without balancing this effect is cumulative.

The combination of cell voltage limits and SOC mismatch ties the pack capacity to the capacity of the weakest cell when discharging and strongest cell when charging. Therefore, charging an imbalanced battery pack results in one or more cells reaching the

maximum voltage charge level before the rest of the cells in the series string. During discharging, the cells that are not fully charged will be depleted before the other cells in the string, causing an early under-voltage shutdown of the pack. These early charge and discharge limits reduce the usable charge in the battery.

Manufactured cell capacities are usually matched within 3% [10]. If Li-Ion cells were not matched in manufacturing, or if cells with differing self-discharge characteristics are allowed to remain on the shelf for long periods prior to pack manufacture, cell voltage differences of 150 mV at full charge are possible. These differences could result in an initial 13% to 18% reduction in battery pack capacity. Even if they are matched by capacity in the factory, the varying cell-to-cell self-discharge rates could reduce the capacity of a pack over time, simply by sitting on the shelf.

Cell balancing techniques can substantially recover this capacity loss, increasing the operating time and pack longevity. An example is shown in Figure 6.1 and Figure 6.2 [10]. If the cells were balanced by applying a differential current to cell #1 during each charge operation, then both cells and the pack would provide full capacity, with only minor loss if not used for a long period.

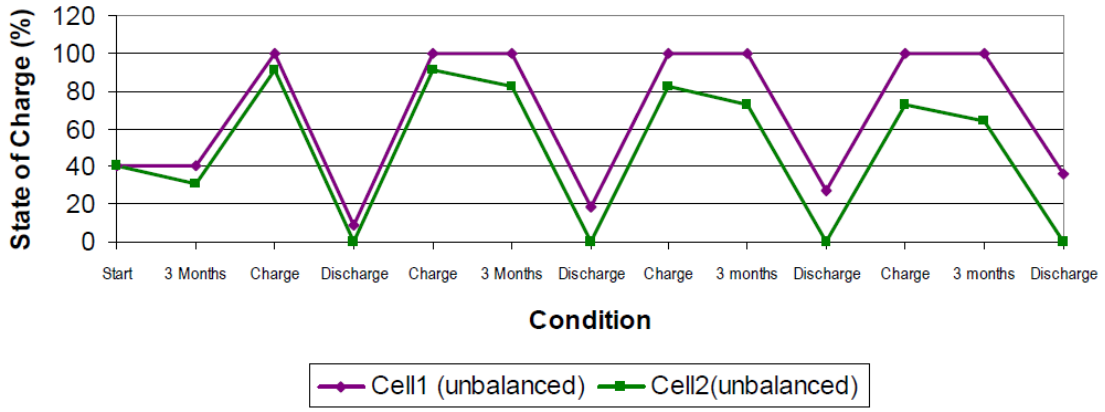

Figure 6.1 SOC mismatch without balancing system

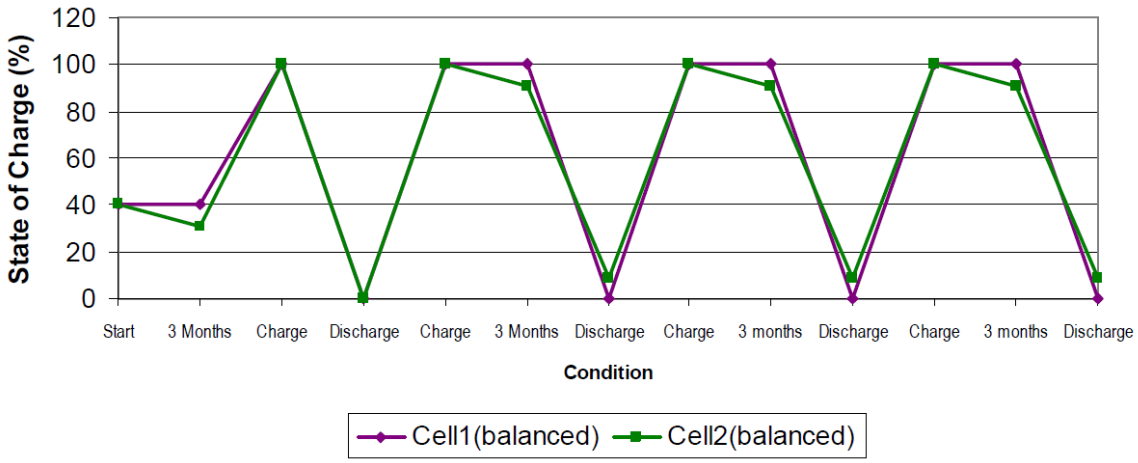

Figure 6.2 SOC mismatch with balancing system

6.2 Capacity Optimization

In this section, an exemplary simulation is implemented in MATLAB according to bi-directional balancing system and predefined battery pack current profile from a standard driving cycle (Schedule A) covered by an EV. Then, the cell balancing problem is formulated in order to determine the optimal current values of each DC/DC converter for that pack current profile to minimize unused capacity. Firstly, several constrains including

minimum and maximum SOC, the current of DC/DC converter i_{dc} and current of individual cell i_c by physical limits need to be considered:

$$\begin{aligned} &SOC_{\min} \le SOC_c(k) \le SOC_{\max} \\ &i_{dc\_\min} \le i_{c,balancing}(k) \le i_{dc\_\max} \\ &i_{c\_\min} \le i_c(k) \le i_{c\_\max} \end{aligned} \tag{6-1}$$

Then, the power losses from the converters of the balancing circuits can be ignored and an approximation of current-balance constrains is made in the problem:

$$\sum_{c=1}^{N} i_{c,balancing} = 0 \tag{6-2}$$

$$i_{pack}(k) = i_c(k) - i_{c,balancing}(k) \tag{6-3}$$

Where $c \in \{1,2...N\}$ represents each of the battery cells of a string made up of N cells and $k \in \{0,1...T\}$ is the current time. Variables $i_{c\_balancing}$ is the single cell balancing current and i_{pack} is the predefined pack current. It shows the net sum of the current injected by balancing circuit in the cells should be zero.

In what follows, our interest in realizing battery pack capacity equalization is given by

$$J_{SOC} = \sum_{c=1}^{N} (SOC_c(t) - \overline{SOC}(t))^2 \tag{6-4}$$

Where $\overline{SOC} = \sum_{c=1}^{N} \frac{SOC_c(t)}{N}$ is the mean SOC of the battery pack. The objective function is to keep every individual cell close to mean SOC as possible as they can.

In conclusion, the defined problem for a discrete finite time horizon (with sample time ΔT=10s) is formulated as follows:

Objective Function:

$$J_{SOC}=\sum_{c=1}^{N}(SOC_c(t)-\overline{SOC}(t))^2, \overline{SOC}=\sum_{c=1}^{N}\frac{SOC_c(t)}{N} \tag{6-5}$$

Minimize:

$$J=J_{SOC} \tag{6-6}$$

Subject to:

$$\begin{aligned}
&SOC(k+1)=SOC(k)-\frac{\Delta T\eta}{Cn}i_c(k) \\
&SOC(0)=SOC_{initial} \\
&\sum_{c=1}^{N} i_{c,balancing}=0,\quad i_{pack}(k)=i_c(k)\text{-}i_{c,balancing}(k) \\
&SOC_{\min}\le SOC_c(k)\le SOC_{\max} \\
&i_{dc_\min}\le i_{c,balancing}(k)\le i_{dc_\max} \\
&i_{c_\min}\le i_c(k)\le i_{c_\max} \\
&c\in\{1,2...N\}, k\in\{0,1...T\}
\end{aligned} \tag{6-7}$$

6.2.1 Simulation Results

The single-objective balancing is applied to an exemplary case, considering an active balancing circuit topology able to provide bi-directional power flow control which has been tested in chapter 4, connected to a battery pack made up of three 5.4Ah Li-ion cells in series. The described methodology is implemented in MATLAB and the formulated

cell balancing problem is solved by “fmincon” function to extract the optimal balancing current for the predefined driving cycle and test the balancing performance.

The parameter configuration of the simulation is shown in Table 6.1 and the simulation results are shown in Figure 6.3-Figure 6.7.

Table 6.1 Simulation Parameter Configuration

Variables	Symbols	Value	Unit
Nominal Capacity	Cn	5.4	Ah
Actual Capacity	Cn1, Cn2, Cn3	5.4/5.1/5.2	Ah
Initial SOC	SOC_init	0.9/0.88/0.87	
SOC Limit	[SOC_min, SOC_max]	[0.05,0.95]	
Cell Current Limit	[I_c_min, I_c_max]	[-50,50]	A
DC/DC Current Limit	[I_{dc}_min, I_{dc} _max]	[-26.5,26.5]	A

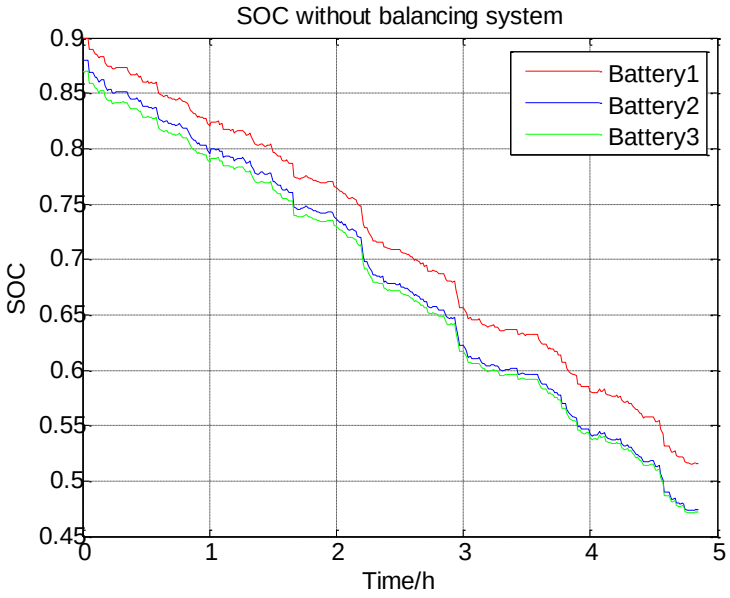

Figure 6.3 SOC without balancing system

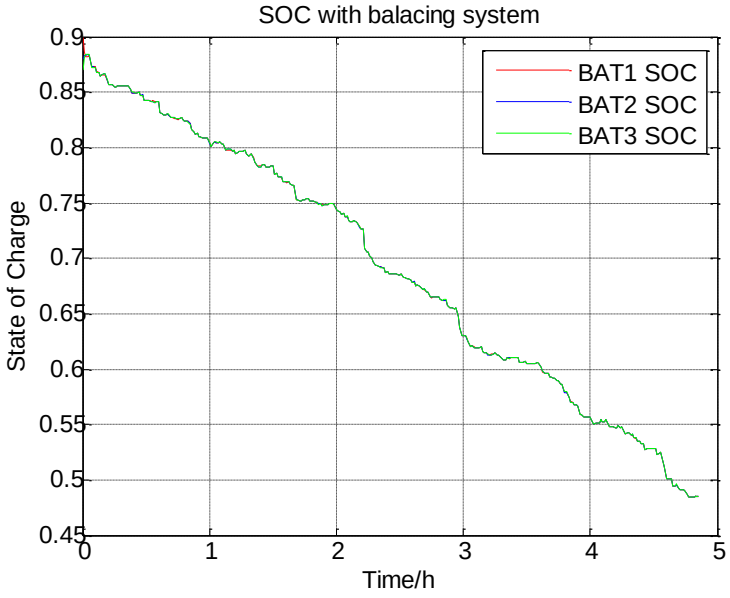

Figure 6.4 SOC with balancing system

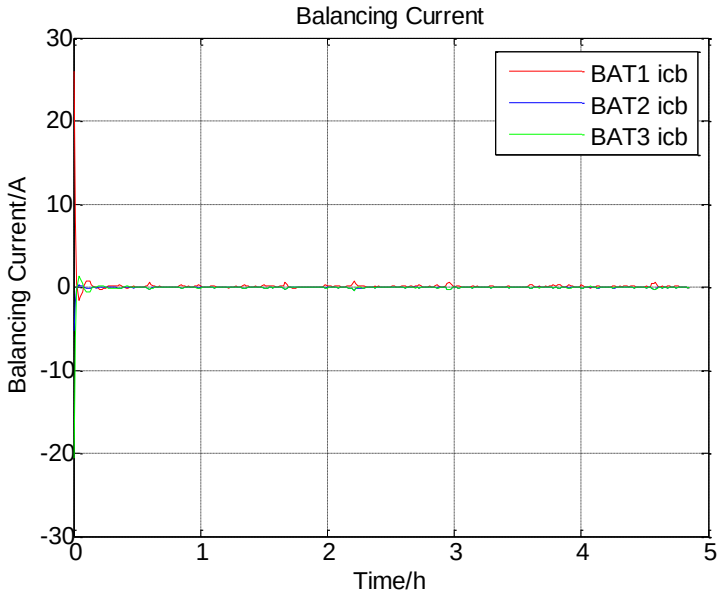

Figure 6.5 Balancing current

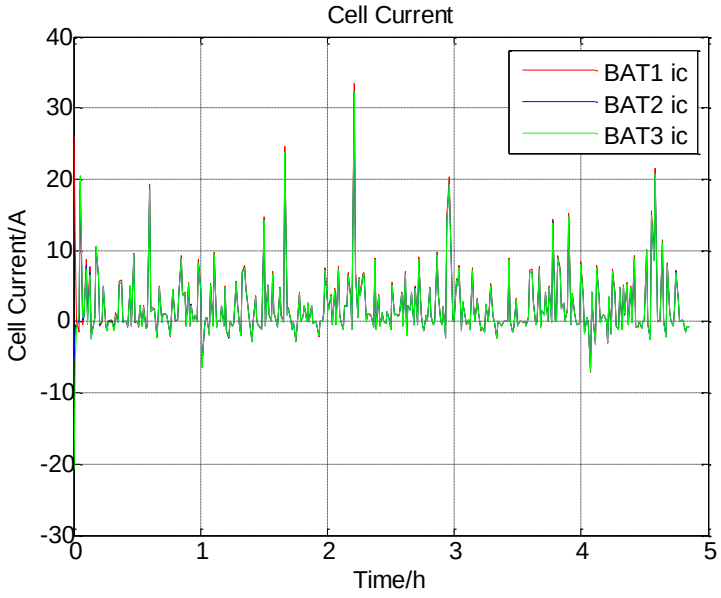

Figure 6.6 Cell current

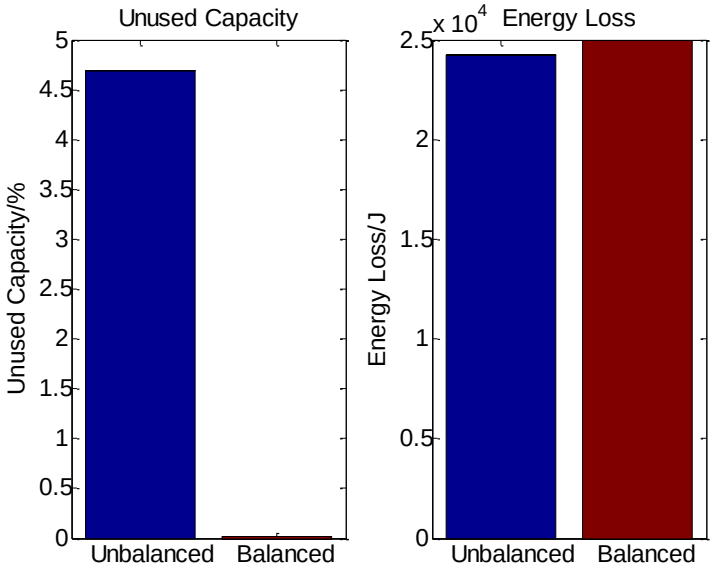

Figure 6.7 Unused capacity & Energy loss

The unused capacity can be defined as: at the end of the cycle, the difference between the maximum and minimum SOC. If any of the weak cells hits the cell under-voltage protection limit while the pack voltage is still sufficient to power the system, the full capacity of the battery will not be used. Therefore, the unused capacity at every cycle will be wasted. Even worse, if the pack is continually being used, overdischarging may occur and result in permanent damages in battery cells. Figure 6.3-Figure 6.7 depicts the simulation results for the predefined driving cycle. It shows a fast and efficient SOC based equalization of the entire battery pack. The unused capacity can be considerably reduced from 4.69% to 0.02%, which means the balancing system can prolong the battery range and help EV to drive farther by using this part of capacity.

However, during balancing process, the energy loss increased significantly due to bringing in balancing system, which is not expected. So in the following section, another

term is brought in the objective function and applied on cell imbalance problem in order to optimize cell unused capacity and energy loss simultaneously.

6.2.2 Energy Loss Reduction

According to [64]–[69], a trade-off needs to be conducted between several targets. In this research, for the purpose of optimizing unused capacity and energy at the same time, another cost penalizes the power loss which can be described as

$$J_{LOSS} = \sum P_{loss} = \sum_{c=1}^{N} R_{bat} i_c(t)^2 \tag{6-8}$$

Where R_{bat} is the battery internal resistance. Note that this penalty only considers the power loss inside of battery and ignores any other loss from the balancing circuit. Therefore, the cell balancing problem can be formulated as different format as

Minimize:

$$J = \int_0^T (PJ_{SOC} + QJ_{LOSS})dt \tag{6-9}$$

Subject to:

$$SOC(k+1) = SOC(k) - \frac{\Delta T \eta}{Cn} i_c(k) \tag{6-10}$$

$$SOC(0) = SOC_{initial}$$

$$\sum_{c=1}^{N} i_{c,balancing} = 0, \quad i_{pack}(k) = i_c(k) - i_{c,balancing}(k)$$

$$SOC_{\min} \le SOC_c(k) \le SOC_{\max}$$

$$i_{dc\_\min} \le i_{c,balancing}(k) \le i_{dc\_\max}$$

$$i_{c\_\min} \le i_c(k) \le i_{c\_\max}$$

$$c \in \{1, 2 \ldots N\}, k \in \{0, 1 \ldots T\}$$

$$P, Q \in \Re^{+}$$

Accomplishing each of the objectives separately leads to different current behaviors. In that sense, in this formulation, a trade-off is required between these objectives. Hence, the weights P and Q are introduced. The weighing variables need to be tuned properly to get reasonable results depended on optimization target. After trial and error, an acceptable simulation result with P=200 and Q=1 is shown in Figure 6.8-Figure 6.11.

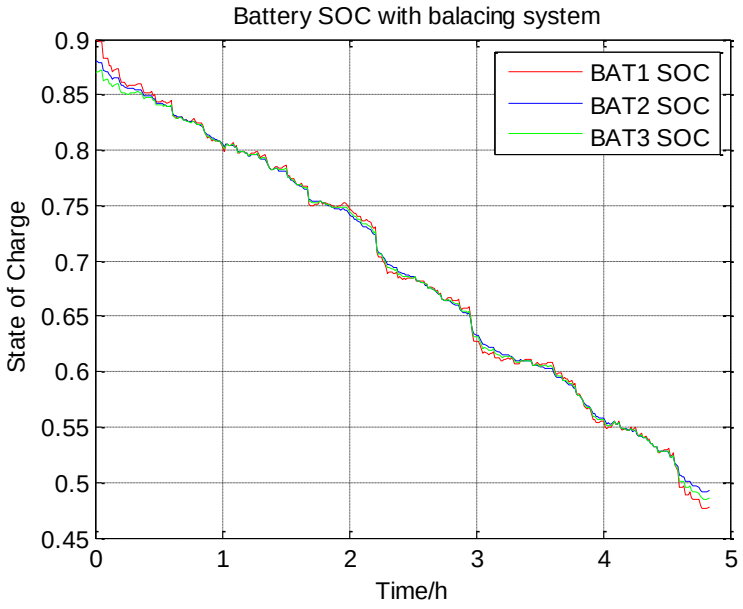

Figure 6.8 SOC with balancing system (P=200, Q=1)

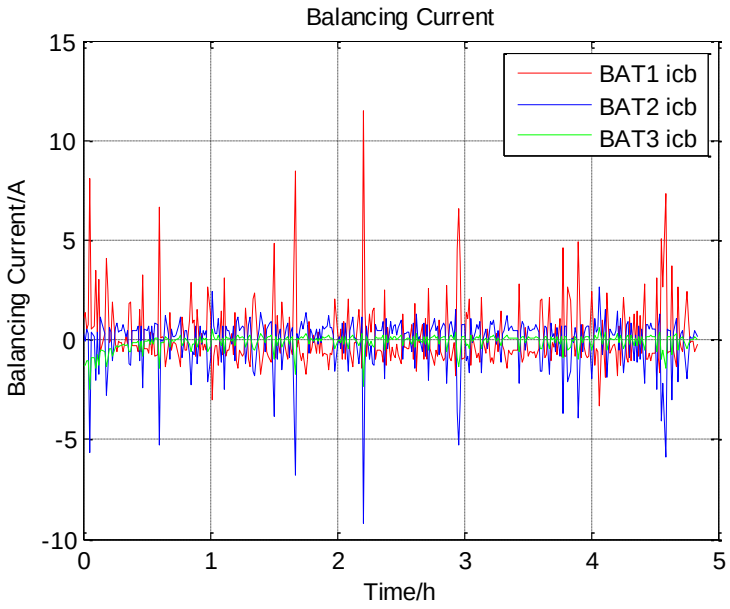

Figure 6.9 Balancing current (P=200, Q=1)

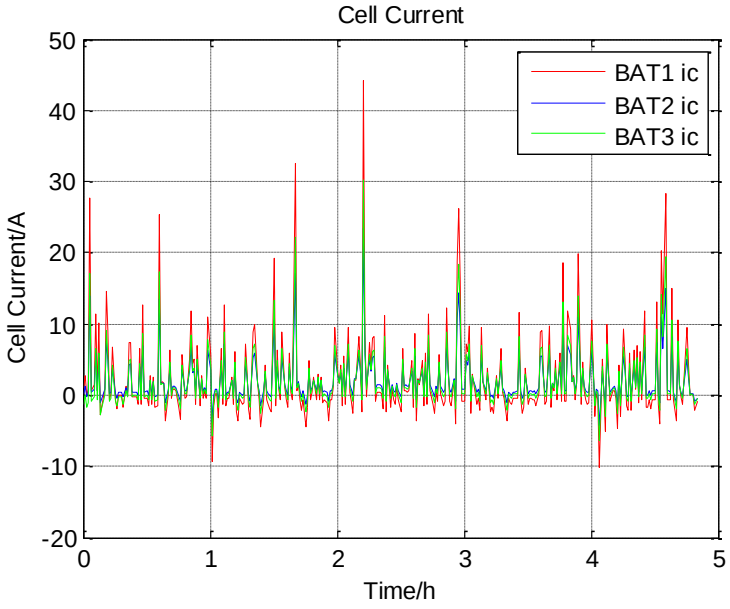

Figure 6.10 Cell current (P=200, Q=1)

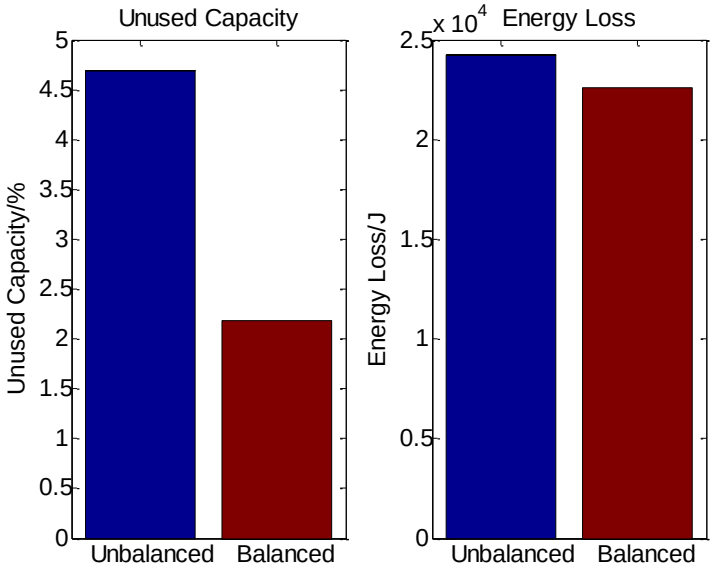

Figure 6.11 Unused capacity & Energy loss (P=200, Q=1)

As discussed above, when applying a larger weighing value, the corresponding objective will have more effect on the cost function and result in different balancing performance. In order to capture a lower energy loss performance, slight single cell SOC equalization could be sacrificed. Under P=200 and Q=1 condition, the optimal balancing current across DC/DC converter can not only reduce unused capacity around 2.5% but also save about 1600J energy from battery heat release. Meanwhile, the optimal balancing current can be directly injected into BMS to apply on a battery pack.

6.3 Thermal Balancing

A balancing circuit could also be used for thermal balancing purposes in order to achieve a more uniform temperature distribution within a battery pack. Under extreme current demands, the battery balancing circuit could increase or decrease single cell

charging or discharging current, injecting or drawing current, or even bypassing a cell. Since heat generation in an electrochemical cell depends on the square value of the current (Joule heating), this could be used to control, up to certain level, heat generation at single cell level.

Since the equilibrium potential of the battery is temperature dependent, the temperature must be resolved dynamically so that it is available for computation of the potential during each time step. The temperature change of the battery can be described as a lumped capacitance model, and the differential equation that governs the temperature of the cell T can be written as follows [70]–[72]:

$$mC_p \frac{dT(t)}{dt} + hA(T(t) - T_{env}) = P_{loss}(t) \quad (6\text{-}11)$$

Where m is the mass of the cell, C_p is the specific heat of the cell, h is the cooling coefficient of the cell external surface to the environment, A is the area of the external surface, T_{env} is the environment temperature and P_{loss} is the internal power loss of the battery. Since battery pack occupies large area in EV, different working positions will make individual cell have different cooling conditions. For instance, if a cell locates in the center of the pack or near motor, more heat may be generated in the surrounding and affect the cell temperature; On the contrary, if a cell works around the pack edge or near cooling system, more heat can be released by convection. Therefore, different cooling coefficients for cells mimic different working conditions in EV. The simulation parameters of lumped capacitance thermal model are configured in Table 6.2 and simulation results for thermal balancing based on the optimized power loss are shown in Figure 6.12 and Figure 6.13.

Table 6.2 Thermal Model Parameters Configuration [70]

Variables	Symbols	Value	Unit
Cell mass	m	41	g
Cooling coefficients	h1/h2/h3	10/5/8	W/m^2K
Cell specific heat	C_p	925	J/kg/K
External surface area	A	0.0043	m^2
Environment temperature	T_{env}	25	℃

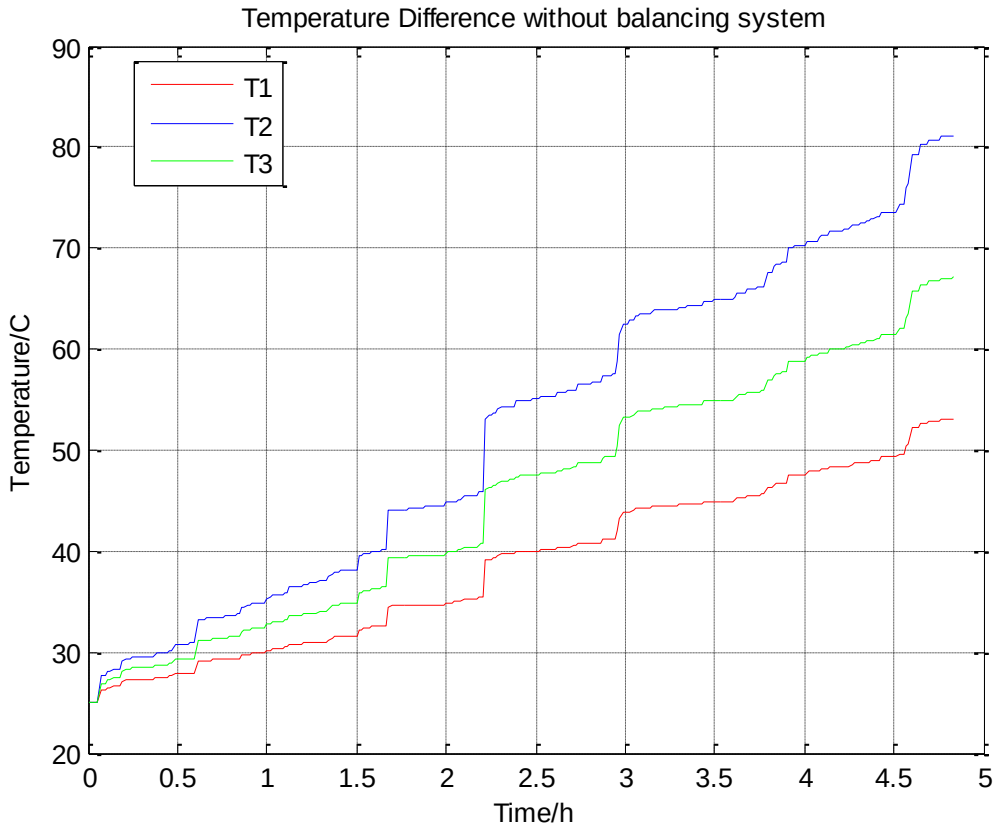

Figure 6.12 Variations of the battery temperature during discharge without balancing system

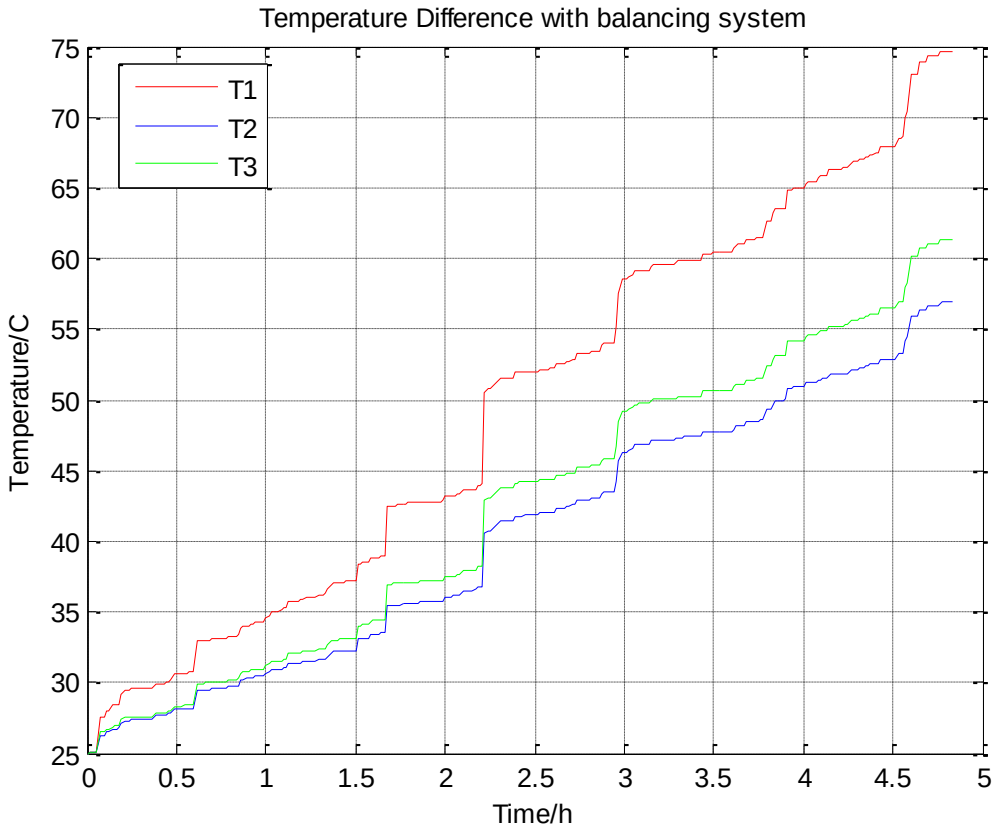

Figure 6.13 Variations of the battery temperature during discharge with balancing system

It is clear that a more uniform temperature distributed among battery pack can be obtained by applying energy reduction term to the objective function. The maximum temperature can be reduced from 81 ℃ down to 74 ℃. Meanwhile, temperature difference inside the pack is decreased from 28 ℃ to 17 ℃. Since battery characteristics is highly depended on temperature, more homogeneous temperature will lead to more united charging and discharging behaviours. Thus, through proposed active cell balancing optimization, cell current can be controlled properly to compensate or dissipate not only

SOC but also thermal effect to prevent further imbalance and then, maximize battery utilization in EV.

Chapter 7 : Conclusion and Future Work

The research presented in this thesis concentrates on advancing the development and implementation of SOC based cell balancing technique on bi-directional power flow system. The experimental electric current input is from a set of real-world mix driving cycles combined with UDDS, US06 and HWFET. The battery combined model is configured by the generated cell-level current profile with the help of GA by taking aging effect into consideration. Furthermore, two estimation strategies, namely EKF and SVSF, are applied on battery fresh (100% capacity) and aged (80% capacity) models. Both EKF and SVSF show high accurate under white Gaussian noise and can converge fast to the actual initial SOC in the very beginning if parameters are configured properly. Essentially, SVSF shows better robustness when facing relatively large model uncertainties. Then, compared with different balancing topologies, “Fly-back” converter can work in bi-directional mode (charging and discharging) and realize battery pack SOC equilibrium in very short time. The performance is quite good for idle and plug-in charge mode due to high credibility SOC value. Based on the previous SOC estimation and bi-directional balancing system, cell balancing can be formulated as an optimal control problem and solved in MATLAB to capture an optimal balancing current for the predefined current profile. The simulation shows cell balancing techniques can not only optimize the unused capacity to expand the battery range but also reduce the energy loss from heat release. More importantly, a more uniform temperature among the pack can be captured and the maximum temperature of the individual cell can be reduced as well.

For the recommendation of the future work, more high-level estimation strategies need to be developed with high fidelity if the noise is not white Gaussian anymore. Also, the time consuming of the sophisticated algorithms needs to be considered as well to ensure realizing real-time estimation on the vehicles.

It is important to note that in the cell balancing implementation, the balancing current is constant and configured by the external resistance. Therefore, it is difficult to control to get the same results as good as the proposed optimization presents. In a word, a changeable balancing current control topology can be more applicable in the EV industries.

The last recommendation for this research involves further study of SOH estimation and balance. Single cell SOC equalization can only balance battery SOC at current driving cycle but it cannot balance battery intrinsic discrepancies. Therefore, cell imbalance problem still exists among the pack and will happen in the future. These discrepancies are temperature depended, and also have a strong link with battery SOH due to capacities divergence. In conclusion, in order to fix cell imbalance problem essentially at present and future, further study on how to balance SOC, temperature, and SOH with accurate estimation strategies needs to be explored.

References

[1] S. Campanari, G. Manzolini, and F. Garcia de la Iglesia, "Energy analysis of electric vehicles using batteries or fuel cells through well-to-wheel driving cycle simulations," *J. Power Sources*, vol. 186, no. 2, pp. 464–477, 2009.

[2] S. Chen, "Extended Kalman Filter Based In-Cylinder Temperature Estimation for Diesel Engines With Thermocouple Lag Compensation," *J. Dyn. Syst. Meas. Control*, vol. 136, no. 51010–1, 2014.

[3] J. Ning and F. Yan, "Nonlinear Disturbance Observer Design for Estimation of Ammonia Storage Ratio in Selected Catalytic Reduction Systems," *Am. Control Conf. (ACC), 2015. IEEE*, 2015.

[4] J. Ning and F. Yan, "Compound Control Strategy Based on Active Disturbance Rejection for Selected Catalytic Reduction systems," *J. Dyn. Syst. Meas. Control*, vol. 137, no. 51008–9, 2015.

[5] J. N. and F. Yan, "Disturbance rejection in DOC-out temperature control for DPF regeneration Disturbance rejection in DOC-out temperature control for DPF regeneration," *Proc. Inst. Mech. Eng. Part D J. Automob. Eng.*, vol. 231.4, no. 487–499., 2016.

[6] G. L. Plett, "Extended Kalman filtering for battery management systems of LiPB-based HEV battery packs Part 1. Background," *J. Power Sources*, vol. 134, no. 2, pp. 252–261, 2004.

[7] H. Rahimi-Eichi, F. Baronti, and M. Y. Chow, "Online adaptive parameter identification and state-of-charge coestimation for lithium-polymer battery cells," *IEEE Trans. Ind. Electron.*, vol. 61, no. 4, pp. 2053–2061, 2014.

[8] Y. Lai, "Analog Applications Journal," *Analog Appl. J.*, no. November, pp. 1069–1072, 2009.

[9] A. C. Baughman and M. Ferdowsi, "Double-Tiered Switched-Capacitor Battery Charge Equalization Technique," *IEEE Trans. Ind. Electron.*, vol. 55, no. 6, pp. 2277–2285, 2008.

[10] Martinez，Carlos, "Cell Balancing Maximizes The Capacity Of Multi-Cell Li-Ion Battery Packs," *Intersil, Inc.*, 2005.

[11] R. Delrossi, "Cell Balancing Design Guidelines," *Microchip Technol. Inc.*, 2002.

[12] S. Wang, L. Shang, Z. Li, H. Deng, and J. Li, "Online dynamic equalization adjustment of high-power lithium-ion battery packs based on the state of balance estimation," *Appl. Energy*, vol. 166, pp. 44–58, 2016.

[13] G. L. Plett, "Extended Kalman filtering for battery management systems of LiPB-based HEV battery packs: Part 2. Modeling and identification," *J. Power Sources*, vol. 134, no. 2, pp. 262–276, 2004.

[14] M. Farag, "Lithium-Ion Batteries : Modelling and State of Charge Estimation," Mechanical Engineering, McMaster University, 2013.

[15] H. Rahimi Eichi and M. Y. Chow, "Modeling and analysis of battery hysteresis

effects," *2012 IEEE Energy Convers. Congr. Expo. ECCE 2012*, pp. 4479–4486, 2012.

[16] X. Hu, S. Li, and H. Peng, "A comparative study of equivalent circuit models for Li-ion batteries," *J. Power Sources*, vol. 198, pp. 359–367, 2012.

[17] R. Ahmed, "Modeling and State of Charge Estimation of Electric Vehicle," Mechanical Engineering, McMaster University, 2014.

[18] C. Speltino, D. Di Domenico, G. Fiengo, and A. Stefanopoulou, "Comparison of Reduced Order Lithium-Ion Battery Models for Control Applications," in *Joint 48th IEEE Conference on Decision and Control and 28th Chinese Control Conference*, 2009, pp. 3276–3281.

[19] R. Ahmed, M. El Sayed, I. Arasaratnam, J. Tjong, and S. Habibi, "Reduced-Order Electrochemical Model Parameters Identification and SOC Estimation for Healthy and Aged Li-Ion Batteries. Part I: Parameterization Model Development for Healthy Batteryies," *IEEE J. Emerg. Sel. Top. Power Electron.*, vol. 2, no. 3, pp. 659–677, 2014.

[20] R. Ahmed, M. El Sayed, I. Arasaratnam, J. Tjong, and S. Habibi, "Reduced-Order Electrochemical Model Parameters Identification and State of Charge Estimation for Healthy and Aged Li-Ion Batteries — Part II : Aged Battery Model and State of Charge Estimation," *IEEE J. Emerg. Sel. Top. POWER Electron.*, vol. 2, no. 3, pp. 678–690, 2014.

[21] R. Ahmed, J. Gazzarri, S. Onori, S. Habibi, R. Jackey, K. Rzemien, J. Tjong, and J. LeSage, "Model-Based Parameter Identification of Healthy and Aged Li-ion Batteries for Electric Vehicle Applications," *SAE Int. J. Altern. Powertrains*, vol. 4, no. 2, pp. 2015-01–0252, 2015.

[22] J. Remmlinger, M. Buchholz, M. Meiler, P. Bernreuter, and K. Dietmayer, "State-of-health monitoring of lithium-ion batteries in electric vehicles by on-board internal resistance estimation," *J. Power Sources*, vol. 196, no. 12, pp. 5357–5363, 2011.

[23] V. Pop, H. J. Bergveld, P. P. L. Regtien, J. H. G. Op het Veld, D. Danilov, and P. H. L. Notten, "Battery Aging and Its Influence on the Electromotive Force," *J. Electrochem. Soc.*, vol. 154, no. 8, p. A744, 2007.

[24] C. Guenther, B. Schott, W. Hennings, P. Waldowski, and M. A. Danzer, "Model-based investigation of electric vehicle battery aging by means of vehicle-to-grid scenario simulations," *J. Power Sources*, vol. 239, pp. 604–610, 2013.

[25] A. T. Stamps, C. E. Holland, R. E. White, and E. P. Gatzke, "Analysis of capacity fade in a lithium ion battery," *J. Power Sources*, vol. 150, no. 1–2, pp. 229–239, 2005.

[26] E. Wood, M. Alexander, and T. H. Bradley, "Investigation of battery end-of-life conditions for plug-in hybrid electric vehicles," *J. Power Sources*, vol. 196, no. 11, pp. 5147–5154, 2011.

[27] J. C. B. Saha, K.Goebel, S.Poll, "An integrated approach to battery health

monitoring using Bayesian regression and state estimation," *autotestcon, 2007 IEEE. Ieee*, pp. 646–653, 2007.

[28] I. Arasaratnam, A. Ryan, E.-S. Mohammed, T. Jimi, and H. Saeid, "Li-Ion Battery SoC Estimation Using a Bayesian Tracker," *SAE Tech. Pap.*, 2013.

[29] W. He, N. Williard, C. Chen, and M. Pecht, "State of charge estimation for electric vehicle batteries using unscented kalman filtering," *Microelectron. Reliab.*, vol. 53, no. 6, pp. 840–847, 2013.

[30] K. S. Ng, C. S. Moo, Y. P. Chen, and Y. C. Hsieh, "Enhanced coulomb counting method for estimating state-of-charge and state-of-health of lithium-ion batteries," *Appl. Energy*, vol. 86, no. 9, pp. 1506–1511, 2009.

[31] B. Pattipati, B. Balasingam, G. V Avvari, and K. R. Pattipati, "Open circuit voltage characterization of lithium-ion batteries," *J. Power Sources*, vol. 269, pp. 317–333, 2014.

[32] F. Huet, "A review of impedance measurements for determination of the state-of-charge or state-of-health of secondary batteries," *J. Power Sources*, vol. 70, pp. 59–69, 1998.

[33] S. Rodrigues, N. Munichandraiah, and A. K. Shukla, "Review of state-of-charge indication of batteries by means of a.c. impedance measurements," *J. Power Sources*, vol. 87, no. 1, pp. 12–20, 2000.

[34] C. Speltino, D. Di Domenico, G. Fiengo, and A. Stefanopoulou, "Experimental

Validation of a Lithium-Ion Battery State of Charge Estimation with an Extended Kalman Filter," in *Control Conference (ECC),2009 European. IEEE,* 2009.

[35] G. L. Plett, "Extended Kalman filtering for battery management systems of LiPB-based HEV battery packs Part 3. State and parameter estimation," *J. Power Sources*, vol. 134, no. 2, pp. 277–292, 2004.

[36] G. L. Plett, "Sigma-point Kalman filtering for battery management systems of LiPB-based HEV battery packs. Part 1: Introduction and state estimation," *J. Power Sources*, vol. 161, no. 2, pp. 1356–1368, 2006.

[37] D. Di Domenico, G. Fiengo, and A. Stefanopoulou, "Lithium-Ion battery State of Charge estimation with a Kalman Filter based on a electrochemical model," in *Control Applications, 2008. CCA 2008. IEEE International Conference on. Ieee,* 2008.

[38] H. Chen, "Adaptive Cubature Kalman Filter for Nonlinear State and Parameter Estimation," in *Information Fusion (FUSION), 2012 15th International Conference on. IEEE*, pp. 1413–1420.

[39] H. Hongwen, X. Rui, Z. Xiaowei, S. Fengchun, and F. JinXin, "State-of-Charge Estimation of the Lithium-Ion Battery Using an Adaptive Extended Kalman Filter Based on an Improved Thevenin Model," *Veh. Technol. IEEE Trans.*, vol. 60, no. 4, pp. 1461–1469, 2011.

[40] S. Habibi, "The Smooth Variable Structure Filter," *Proc. IEEE*, vol. 95, no. 5, 2007.

[41] H. H. Afshari and R. Ahmed, "State of Charge Estimation of Li-Ion Batteries Using the Dynamic 2nd Order Smooth Variable Structure Filter," in *25th CANCAM*, 2015.

[42] S. W. Moore and P. J. Schneider, "A Review of Cell Equalization Methods for Lithium Ion and Lithium Polymer Battery Systems," *SAE Tech. Pap.*, no. 2001-01–0959, 2001.

[43] J. Cao, N. Schofield, and A. Emadi, "Battery balancing methods: A comprehensive review," *2008 IEEE Veh. Power Propuls. Conf. VPPC 2008*, pp. 3–8, 2008.

[44] M. Daowd, N. Omar, P. Van Den Bossche, and J. Van Mierlo, "Passive and Active Battery Balancing comparison based on MATLAB Simulation," in *Vehicle Power and Propulsion Conference (VPPC), 2011 IEEE. IEEE*, 2011.

[45] W. C. Lee, D. Drury, and P. Mellor, "Comparison of Passive Cell Balancing and Active Cell Balancing for Automotive Batteries," *Veh. Power Propuls. Conf. (VPPC), 2011 IEEE. IEEE*, 2011.

[46] A. Najmabadi, "Evaluation of Active Balancing Algorithms and an Improved Method for a Deployed Active Battery Balancer as Well as Physical Implementation," Mechanical Engineering, McMaster University, 2002.

[47] K. G.A., "Switched-capacitor systems for battery equalization," *Mod. Tech. Technol. 2000. MTT 2000. Proc. VI Int. Sci. Pract. Conf. Students, Post-graduates Young Sci. IEEE*, pp. 57–59, 2000.

[48] C. Pascual and P. T. Krein, "Switched capacitor system for automatic series battery

equalization," *Proc. APEC 97 - Appl. Power Electron. Conf.*, vol. 2, pp. 848–854, 1997.

[49] M. Kim, S. Member, C. Kim, S. Member, J. Kim, S. Member, and G. Moon, "A Chain Structure of Switched Capacitor for Improved Cell Balancing Speed of Lithium-Ion Batteries," *IEEE Trans. Ind. Electron.*, vol. 61, no. 8, pp. 3989–3999, 2014.

[50] Y. Yuanmao, K. W. E. Cheng, S. Member, and Y. P. B. Yeung, "Zero-Current Switching Switched-Capacitor Zero-Voltage-Gap Automatic Equalization System for Series Battery String," *IEEE Trans. POWER Electron.*, vol. 27, no. 7, pp. 3234–3242, 2012.

[51] W. Hong, K. S. Ng, J. H. Hu, and C. S. Moo, "Charge equalization of battery power modules in series," *2010 Int. Power Electron. Conf. - ECCE Asia -, IPEC 2010*, pp. 1568–1572, 2010.

[52] T. Gottwald, Z. Ye, and T. Stuart, "Equalization of EV and HEV batteries with a ramp converter," *IEEE Trans. Aerosp. Electron. Syst.*, vol. 33, no. 1, pp. 307–312, 1997.

[53] M. Einhorn, S. Member, W. Roessler, and J. Fleig, "Improved Performance of Serially Connected Li-Ion Batteries With Active Cell Balancing in Electric Vehicles," *IEEE Trans. Veh. Technol.*, vol. 60, no. 6, pp. 2448–2457, 2011.

[54] M. Hagiwara and H. Akagi, "Control and Experiment of Pulsewidth-Modulated

Modular Multilevel Converters," *IEEE Trans. POWER Electron.*, vol. 24, no. 7, pp. 1737–1746, 2009.

[55] W. Huang and J. A. A. Qahouq, "Energy Sharing Control Scheme for State-of-Charge Balancing of Distributed Battery Energy Storage System," *IEEE Trans. Ind. Electron.*, vol. 62, no. 5, pp. 2764–2776, 2015.

[56] W. C. Lee and D. Drury, "Development of a Hardware-in-the-Loop Simulation System for Testing Cell Balancing Circuits," *IEEE Trans. POWER Electron.*, vol. 28, no. 12, pp. 5949–5959, 2013.

[57] Y. Lee and M. Cheng, "Intelligent Control Battery Equalization for Series Connected Lithium-Ion Battery Strings," *IEEE Trans. Ind. Electron.*, vol. 52, no. 5, pp. 1297–1307, 2005.

[58] J. R. Belt, "Battery Test Manual for Plug-In Hybrid Electric Vehicles," *Idaho Natl. Lab.*, no. INL/EXT-07-12536, 2010.

[59] D. E. Goldberg, *Genetic Algorithms in Search , Optimization , and Machine Learning*. 1989.

[60] S. Andrew Gadsden, S. R. Habibi, and T. Kirubarajan, "The smooth particle variable structure filter," *Trans. Can. Soc. Mech. Eng.*, vol. 36, no. 2, pp. 177–193, 2012.

[61] G. S.A., "Smooth variable structure filtering: theory and applications," Mechanical Engineering, McMaster University, 2011.

[62] A. I. Pressman, *Switching Power Supply Design*. McGraw-Hill, Inc., 1997.

[63] L. T. Corporation, “LTC3300-1 - High Efficiency Bidirectional Multicell Battery Balancer (Datasheet),” pp. 1–46, 2013.

[64] J. Varela, D. Castro, and J. V Barreras, “Multi-Objective Control of Balancing Systems for Li-Ion Battery Packs : A paradigm shift ?,” in *Vehicle Power and Propulsion Conference (VPPC), 2014 IEEE. IEEE*, 2014.

[65] S. J. Moura, D. S. Callaway, H. K. Fathy, and J. L. Stein, “Tradeoffs between battery energy capacity and stochastic optimal power management in plug-in hybrid electric vehicles,” *J. Power Sources*, vol. 195, pp. 2979–2988, 2010.

[66] B. Lunz, Z. Yan, J. Bernhard, and D. Uwe, “Influence of plug-in hybrid electric vehicle charging strategies on charging and battery degradation costs,” *Energy Policy*, vol. 46, pp. 511–519, 2012.

[67] N. Bouchhima, M. Schnierle, S. Schulte, and K. Peter, “Active model-based balancing strategy for self-recon fi gurable batteries,” *J. Power Sources*, vol. 322, pp. 129–137, 2016.

[68] S. Bashash, S. J. Moura, J. C. Forman, and H. K. Fathy, “Plug-in hybrid electric vehicle charge pattern optimization for energy cost and battery longevity,” *J. Power Sources*, vol. 196, no. 1, pp. 541–549, 2011.

[69] Z. Yu, D. Zinger, and A. Bose, “An innovative optimal power allocation strategy for fuel cell , battery and supercapacitor hybrid electric vehicle,” *J. Power Sources*, vol. 196, no. 4, pp. 2351–2359, 2011.

[70] L. Gao, S. Liu, R. A. Dougal, and S. Member, "Dynamic lithium-ion battery model for system simulation," *Components Packag. Technol. IEEE Trans.*, vol. 25, no. 3, pp. 495–505, 2002.

[71] X. Lin, H. E. Perez, J. B. Siegel, A. G. Stefanopoulou, Y. Li, R. D. Anderson, Y. Ding, and M. P. Castanier, "Online Parameterization of Lumped Thermal Dynamics in Cylindrical Lithium Ion Batteries for Core Temperature Estimation and Health Monitoring," *IEEE Trans. Control Syst. Technol.*, vol. 21, no. 5, pp. 1745–1755, 2013.

[72] A. A. Pesaran, "Battery thermal models for hybrid vehicle simulations," *J. Power Sources*, no. 110.2, pp. 377–382, 2002.